

ROCKGLACIER KINEMATICS IN A HIGH MOUNTAIN GEOSYSTEM

Dissertation

zur

Erlangung des Doktorgrades (Dr. rer. nat.)

der

Mathematisch-Naturwissenschaftlichen Fakultät

der

Rheinischen Friedrich-Wilhelms-Universität Bonn

vorgelegt von

Isabelle Roer

aus

Bonn

Bonn, Februar 2005

Angefertigt mit Genehmigung der Mathematisch -Naturwissenschaftlichen Fakultät der
Rheinischen Friedrich-Wilhelms-Universität Bonn

1. Referent: Prof. Dr. R. Dikau
2. Referent: PD Dr. A. Käab

Tag der Promotion: 03.06.2005

*I dedicate this in loving memory to my father
and with warm thanks to my mother.*



View into the Rothorn-cirque (Hungerlitälli), Brunegghorn (3833 m a.s.l.) and Bishorn (4134 m a.s.l.) in the back.

SUMMARY

The study presents a regional approach for the quantification of rockglacier creep in a high mountain geosystem (Turtmann valley, Swiss Alps).

By a combination of different methods, rockglacier movements were analysed qualitatively and quantitatively on various spatial and temporal scales. The application of digital photogrammetry and terrestrial geodetic survey enabled the quantification of horizontal velocities and vertical changes. The photogrammetric results demonstrate that small-scale aerial photographs are highly useful to measure changes in rockglacier geometry. Also the combination with high resolution imagery (from HRSC-A), which was applied for the first time in rockglacier studies, has been successful. Thus, displacements were investigated in a large area (meso-scale) and over a time span of 26 years (1975 – 2001). Against that, terrestrial geodetic survey enabled the annual quantification of block displacements on two rockglaciers between 2001 and 2004. The first-time application of dendrogeomorphic techniques for the determination of permafrost creep provided preliminary results for two rockglaciers.

The applied techniques and especially the combination of geomorphic mapping and digital photogrammetry allowed the reliable assessment of the state of activity for 45 rockglaciers. Horizontal and vertical surface changes were analysed on 34 rockglaciers and a clear activity was revealed on 18 of them. Most of the permafrost bodies indicated above-average horizontal velocities compared to other rockglaciers in the Alps. In addition, conspicuous spatio-temporal variations in horizontal velocities and vertical changes were observed. Regarding the temporal variations, a distinct increase in horizontal velocity – probably from the beginning of the 1990s – was ascertained for all investigated active rockglaciers.

The described findings were discussed by consideration of probable controls, such as terrain parameters and climatic influences. Although the data on decisive forcing factors and the knowledge on rockglacier dynamics is limited, it is assumed that the observed speed-up is linked to climatic changes and an increase in ground temperatures, respectively. Thus, the investigated kinematics supports the role of rockglaciers as sensitive indicators for changes in the high mountain geosystem.

ZUSAMMENFASSUNG

Im Zentrum der hier vorgestellten Studie steht die regionale Analyse der Blockgletscherbewegung in einem hochalpinen Geosystem (Turtmantal, Schweizer Alpen).

Mit Hilfe mehrerer Methoden wurde die Blockgletscherkinematik auf unterschiedlichen Raum- und Zeitskalen sowohl qualitativ als auch quantitativ untersucht. Die Anwendung der digitalen Photogrammetrie und der terrestrischen Vermessung ermöglichte die Messung von horizontalen Geschwindigkeiten und vertikalen Veränderungen. Dabei zeigten die Ergebnisse der Photogrammetrie, dass analoge hochgeflogene Luftbilder für die Analyse von Veränderungen der Blockgletschergeometrie durchaus geeignet sind. Auch die Kombination mit digitalen hochauflösenden Daten (der High Resolution Stereo Camera – Airborne; HRSC-A), die erstmalig in der Blockgletscherforschung eingesetzt wurden, war erfolgreich. Dadurch konnten Blockgletscherbewegungen auf großer räumlicher Skala (Mesoskala) und über einen Zeitraum von 26 Jahren (1975 – 2001) quantifiziert werden. Die Anwendung der terrestrischen Vermessung ermöglichte zusätzlich die jährliche Quantifizierung von Bewegungen zwischen 2001 und 2004 auf zwei ausgewählten Blockgletschern. Dendrogeomorphologische bzw. holzanatomische Techniken wurden erstmalig für die Bestimmung der Blockgletscherkinematik eingesetzt und lieferten für zwei Untersuchungsobjekte vorläufige Ergebnisse.

Mit den verwendeten Methoden und besonders durch die Kombination von geomorphologischer Kartierung und digitaler Photogrammetrie konnte der Aktivitätsgrad von 45 Blockgletschern abgeschätzt werden. Horizontale und vertikale Bewegungen wurden dann für die 34 intakten Blockgletscher quantifiziert, von denen 18 eine eindeutige Aktivität zeigten. Viele der untersuchten Permafrostkörper wiesen, im Vergleich zu anderen Blockgletschern der Alpen, überdurchschnittliche horizontale Geschwindigkeiten auf. Außerdem zeigten sowohl die horizontalen als auch die vertikalen Bewegungen deutliche raum-zeitliche Variationen. Bezüglich der zeitlichen Variationen wurde für alle aktiven Blockgletscher eine eindeutige Zunahme der horizontalen Geschwindigkeit – vermutlich ab den 1990er Jahren – bestimmt.

Die geschilderten Ergebnisse wurden unter Einbezug möglicher Kontrollgrößen, wie Relief- und Klimaparametern, diskutiert. Obwohl die Datenlage zu entscheidenden Einflussgrößen und das Wissen über Blockgletscherdynamik limitiert ist, wurde die beobachtete Beschleunigung den klimatischen Veränderungen und dem damit verbundenen Anstieg der Oberflächentemperatur zugewiesen. Folglich stützen die Ergebnisse die Rolle von Blockgletschern als sensitive Indikatoren für Veränderungen im hochalpinen Geosystem.

CONTENTS

SUMMARY

ZUSAMMENFASSUNG

LIST OF FIGURES

I

LIST OF TABLES

XI

ACRONYMS

XII

1	INTRODUCTION	1
1.1	Motivation	1
1.2	Objectives	1
1.3	Conceptual background	2
2	SCIENTIFIC BACKGROUND	5
2.1	High mountain geosystems	5
2.1.1	Definition & characteristics	5
2.1.2	High mountain geomorphology	6
2.2	Periglacial & Permafrost	7
2.2.1	Definition & characteristics	7
2.2.2	Influencing factors	8
2.2.3	Prospecting methods	9
2.2.4	Permafrost distribution, modelling & sensitivity	9
2.3	Rockglaciers	11
2.3.1	History of rockglacier research	11
2.3.2	Rockglacier origin & nomenclature	11
2.3.3	Rockglacier definition	12
2.3.4	Rockglacier distribution, morphology & stratigraphy	12
2.3.5	Rockglacier kinematics	20
2.3.5.1	Rockglacier movement	20
2.3.5.2	Spatial variation of movement (surface & depth)	21
2.3.5.3	Temporal variation of movement (surface & depth)	22
2.3.5.4	Rockglacier rheology	24
2.3.5.5	Methods to monitor rockglacier kinematics	30
3	METHODS	32
3.1	Geomorphic mapping	32
3.2	Digital photogrammetry	32
3.2.1	Basic principles	32
3.2.2	Data	34
3.2.2.1	Aerial photography	34
3.2.2.2	HRSC-A data	34
3.2.3	DTM & orthophoto generation	36
3.2.4	Measurement of horizontal velocities	38
3.2.5	Computation of thickness changes	41
3.3	Terrestrial geodetic survey	44
3.3.1	Total station	44
3.3.2	Measurement design	46
3.4	Dendrogeomorphology	50
3.4.1	Basic principles	50
3.4.2	Measurement design	51
3.5	Temperature monitoring	53
3.5.1	Basic principles	53
3.5.2	Measurement design	54
3.6	Summary	54

4	STUDY SITE	55
4.1	General characteristics	55
4.2	Geology	57
4.3	Climate	58
4.4	Geomorphology	60
5	RESULTS	62
5.1	Geomorphic mapping	62
5.1.1	Hungerlitälli	63
5.1.2	Grüobtälli	66
5.1.3	Niggelingtälli	69
5.1.4	Chummetjitälli	72
5.1.5	Brändjitälli	75
5.1.6	Pipjitälli	77
5.1.7	Summary	79
5.2	Digital photogrammetry	81
5.2.1	Pipjitälli	81
5.2.1.1	Rockglacier Pipp1	81
5.2.1.2	Rockglacier Pipp2	85
5.2.1.3	Rockglacier Pipp3	85
5.2.1.4	Rockglacier Pipp4	85
5.2.1.5	Rockglacier Pibw	87
5.2.2	Brändjitälli	90
5.2.2.1	Rockglacier Brho1	90
5.2.2.2	Rockglacier Brho2	93
5.2.2.3	Rockglacier Brle	93
5.2.3	Hungerlitälli	95
5.2.3.1	Rockglacier Hufh	95
5.2.3.2	Rockglacier Hujp	98
5.2.3.3	Rockglacier Hurh1	101
5.2.3.4	Rockglacier Hurh2	101
5.2.3.5	Rockglacier Huhh1	101
5.2.3.6	Rockglacier Huhh2	105
5.2.3.7	Rockglacier Huhh3	108
5.2.4	Grüobtälli	113
5.2.4.1	Rockglacier Grueo1	113
5.2.4.2	Rockglacier Grueo2	123
5.2.4.3	Rockglacier Grueo3	126
5.2.4.4	Rockglacier Grueo4	129
5.2.4.5	Rockglacier Grueo5	132
5.2.4.6	Rockglacier Grueo6	132
5.2.4.7	Rockglacier Grueo7	136
5.2.4.8	Rockglacier Grueo8	139
5.2.5	Niggelingtälli	140
5.2.5.1	Rockglacier Niggel1	140
5.2.5.2	Rockglacier Niggel2	143
5.2.5.3	Rockglaciers Niggel3-7	146
5.2.6	Chummetjitälli	147
5.2.6.1	Rockglacier Chummet1	147
5.2.6.2	Rockglaciers Chummet2-4	150
5.2.7	Summary	151
5.3	Terrestrial geodetic survey	155
5.3.1	Rockglacier Huhh1	155

5.3.2	Rockglacier Huhh3	166
5.3.3	Summary	174
5.4	Dendrogeomorphology	176
5.4.1	Reaction wood in <i>Pinus cembra</i> stem	176
5.4.2	Anatomical variations in <i>Salix helvetica</i> roots	177
5.5	Temperature monitoring	180
5.5.1	Rockglacier Huhh1	180
5.5.2	Rockglacier Huhh3	181
5.5.3	Rockglacier Hurh2	182
5.5.4	Rockglacier Huhh2	182
5.5.5	Summary	183
6	DISCUSSION	185
7	CONCLUSIONS	199
8	PERSPECTIVES	201
9	ACKNOWLEDGEMENTS	203
10	BIBLIOGRAPHY	204

APPENDICES

Appendix 1A	Published data on horizontal velocities	i
Appendix 1B	Published data on vertical changes	xiii
Appendix 1C	Published data on front advance	xv
Appendix 2	Rockglacier activity (comparison of methods)	xvii
Appendix 3	Pipjitälli 1975-1993 annual horizontal velocity (m/a)	xix
	Pipjitälli 1993-2001 annual horizontal velocity (m/a)	xx
	Brändjitälli 1975-1993 annual horizontal velocity (m/a)	xxi
	Brändjitälli 1993-2001 annual horizontal velocity (m/a)	xxii
	Hungerlitälli 1975-1993 annual horizontal velocity (m/a)	xxiii
	Hungerlitälli 1993-2001 annual horizontal velocity (m/a)	xxiv
	Grüobtälli 1975-1993 annual horizontal velocity (m/a)	xxv
	Grüobtälli 1993-2001 annual horizontal velocity (m/a)	xxvi

LIST OF FIGURES

CHAPTER 1

Figure 1.1: Hierarchical level and size of relief units (modified, after Dikau 1989). Bold face indicates relief units considered in this study.

CHAPTER 2

Figure 2.1: Some basic elements of high mountain landforms (modified, after Barsch & Caine 1984). Black lines and type: glacial erosive forms; grey lines and type: postglacial accumulative forms.

Figure 2.2: Schematic mean annual temperature profile through the surface boundary layer, showing the relation between air temperature and permafrost temperature (modified, after Smith & Riseborough 2002: 5). MAAT = Mean Annual Air Temperature; MAGST = Mean Annual Ground Surface Temperature; T_{TOP} = mean annual Temperature at the Top Of Permafrost.

Figure 2.3: Model of the development of talus rockglaciers (below mountain talus slopes) in discontinuous mountain permafrost environments (from Barsch 1996: 186).

Figure 2.4: Model of the development of a debris rockglacier in mountain permafrost environments (from Barsch 1996: 187).

Figure 2.5: Internal structure of the Muragl rockglacier (from Arenson et al. 2002: 122).

Figure 2.6: Schematic profiles of active, inactive and relict rock glaciers (from Ikeda & Matsuoka 2002: 158).

Figure 2.7: Model of inactive rockglaciers. A: Model of a climatic inactive rockglacier. B: Model of a dynamic inactive rockglacier (from Barsch 1996: 193).

Figure 2.8: Talus rockglacier in discontinuous permafrost at Grüeobtälli (Turtmann valley, Switzerland). Underlying orthophoto of 20.08.1993 (flight-line 16, aerial photographs taken by Swisstopo). Plait-like ridge and furrow topography in the upper part of the rockglacier seems to result from sediment input of two different source areas.

Figure 2.9: Debris rockglacier in discontinuous permafrost at Pipjitälli (Turtmann valley, Switzerland). Underlying orthophoto of 20.08.1975 (flight-line 22, aerial photographs taken by Swisstopo). Former lateral moraines form the margins of the rockglacier.

Figure 2.10: Talus rockglacier in continuous permafrost at Templet (western Svalbard Archipelago, Norway). Photograph taken in September 2004.

Figure 2.11: Rockglacier sequence in the Hungerlitälli (Turtmann valley, Switzerland); A = active, Ia = inactive and R = relict. Underlying orthophoto of 20.08.1975 (flight-line 22, aerial photographs taken by Swisstopo).

Figure 2.12: Horizontal downslope borehole deformation. a) Mutèl-Corvatsch, borehole 2/1987: 1987-1995; b,c) Pontresina-Schafberg, boreholes 1/1990 and 2/1990: 1991-2000, 1994-1999; d, e) Muragl, boreholes 3/1999 and 4/1999: 1999-2000 (from Arenson et al. 2002: 124).

Figure 2.13: Components of rockglacier movement: internal deformation (v^d), sliding (v^s) and deformation at the base (v^u), which are reflected in the surface velocity (v^s) (from Kääb 1996: 65). Sliding and deformation at the base are subsumed into basal velocity (v^b).

- Figure 2.14:** Conceptual model of the parameters affecting the deformation of ice-saturated mountain permafrost bodies (from Barsch 1996: 169).
- Figure 2.15:** Change in surface elevation: A) resulting from a change in mass balance; divergence of flow = 0. B) resulting from a change in flow balance; mass balance = 0. (from: <http://www.geo.unizh.ch/~kaeaeb/e&mhtml/kinbed.html>).
- Figure 2.16:** Influence of a narrowed cross-section on the divergence of the flow and a change in surface elevation (from <http://www.geo.unizh.ch/~kaeaeb/e&mhtml/kinbed.html>).
- Figure 2.17:** Influence of a change in velocity on the divergence of flow and a change in surface elevation (from <http://www.geo.unizh.ch/~kaeaeb/e&mhtml/kinbed.html>).
- Figure 2.18:** Longitudinal profile of rockglacier surface, surface velocities and derived kinematic quantities 1987-1996. The photogrammetric profile measurements have a spatial resolution of 1 m. Surface topography depicted with two times exaggeration. Small scale topography is defined as difference between surface topography at each point and a running average over 200 m (four times exaggeration). (from Käab et al. 1998: 534).

CHAPTER 3

- Figure 3.1:** Principle of photogrammetric DTM generation from a monotemporal stereo model composed of two overlapping images taken from different positions (from Käab 2004: 23). c = focal length; r_{xy} = the horizontal (radial) distance of a terrain point from the sensor nadir; r'_{xy} = radial distance between the image centre and the projection of a terrain point into the image. $\hat{\epsilon}$, \hat{o} and \hat{u} are the rotation angles, decisive for the exterior orientation of the images. The terrain point P is determined by the intersection of oriented rays, fixed by the known projection centres (O_1 , O_2) and the projections (P'_1 , P'_2).
- Figure 3.2:** Processing schema for digital measurement of rockglacier flow-fields (from Roer et al. 2005). Comparison of different input data, processing steps and resulting output data using analogue aerial photographs and digital aerial images. The ellipses mark steps, where the operator can influence the processing to increase the quality of the output data.
- Figure 3.3:** Schema of measuring surface displacements from repeated digital orthoimages by block-correlation techniques (from Käab & Vollmer 2000: 319). A reference block in the orthoimage at time 1 is searched for in a test area in the orthoimage at time 2. The horizontal shift between the reference-block location and corresponding test block gives the surface displacement.
- Figure 3.4:** Annual horizontal displacements (raw data) on rockglacier Grueo1 between 1993 and 2001 (underlying orthoimage of 2001). Due to major changes on the surface in the lower part of the rockglacier, there is a strong loss of coherence resulting in a chaotic vector field, while snow patches and shadows inhibited the measurement of displacement vectors in the root zone.
- Figure 3.5:** Main processing steps for the generation of DTMs and orthophotos (A), horizontal velocities (B) and the computation of thickness changes (C) (modified, after Vollmer 1999).
- Figure 3.6:** Instrument errors of a total-station. A = vertical axis tilt; B = height-index error (i) (V index); C = line-of-sight error (c) (Hz collimation); D = tilting-axis error (a) (from Zeiske 2000: 25).
- Figure 3.7:** Total-station on one of the reference points situated on a latepleistocene moraine with an overview of the research object (rockglacier in the background).
- Figure 3.8:** Steel dowels were drilled into the blocks for high-accuracy re-measurement. The thread, where the prism can directly be screwed into for the measurement, is protected by a plastic screw throughout the year.

Figure 3.9: Terrestrial geodetic survey in the Hungerlitälli: reference and observation points. Underlying orthoimage of 20.08.1975 (flight-line 22, aerial photographs taken by Swisstopo).

Figure 3.10: *Salix helvetica* shrub taken from rockglacier Grueo1. White rectangles (1 and 2) indicate the positions of the taken root samples for the analysis of anatomical variations.

Figure 3.11: Digital micro photo (40x magnification) of a lateral root micro slide showing annual rings and the surrounding bark. Shrub-ID: Isa_W04 (*Salix helvetica*).

CHAPTER 4

Figure 4.1: Location of the Turtmann valley (square in Figure C) within the Valais (© Luzi Bernhard, WSL), Switzerland and the Alps (<http://www.scilands.de>).

Figure 4.2: Shaded relief visualisation of the Turtmann valley and impressions of different subsystems. The numbers and arrows in the map mark the corresponding photograph and its direction of sight.

Figure 4.3: Geological profile through the Valais Alps with the position of the study site (Labhart 1998: 94, modified).

Figure 4.4: Tectonic map of the middle and upper Penninic in the southern Valais (Sartori 1990, modified).

Figure 4.5: Mean annual precipitation values (1971 – 1990, corrected) in the Valais (Hydrologischer Atlas der Schweiz 2001, © Bundesamt für Landestopographie). The white rectangle marks the study area.

CHAPTER 5

Figure 5.1: Orographic right side of the Turtmann valley with investigated hanging valleys (Tällis). Underlying DTM of 2001.

Figure 5.2: Geomorphological map of the Hungerlitälli (from Roer 2003). Legend based on Kneisel et al. (1998). Basic map: Pixelkarte 1:25.000 (© Swiss Federal Office of Topography).

Figure 5.3: Rockglacier occurrence and activity in the Hungerlitälli. Red line = active rockglacier, yellow line = inactive rockglacier, green line = relict rockglacier. Given numbers correspond to the inventory table (table 5.1). Underlying orthophoto of 20.08.1975 (flight-line 22, aerial photographs taken by Swisstopo).

Figure 5.4: Vertical surface changes in the Hungerlitälli between 1975 and 2001 (DTM comparison).

Figure 5.5: Rockglacier occurrence and activity in the Grüobtälli. Red line = active rockglacier, yellow line = inactive rockglacier, green line = relict rockglacier. Given numbers correspond to the inventory table (table 5.2). Underlying orthophoto of 20.08.1975 (left) and 6.10.1975 (right) (flight-line 22 (left), 21 (right); aerial photographs taken by Swisstopo).

Figure 5.6: Vertical surface changes in the Grüobtälli between 1975 and 2001 (DTM comparison).

Figure 5.7: Rockglacier occurrence and activity in the Niggelingtälli. Red line = active rockglacier, yellow line = inactive rockglacier, green line = relict rockglacier. Given numbers correspond to the inventory table (table 5.3). Underlying orthophoto of 11.08.1993 (flight-line 20, aerial photographs taken by Swisstopo).

Figure 5.8: Vertical surface changes in the Niggelingtälli between 1975 and 2001 (DTM comparison).

- Figure 5.9:** Rockglacier occurrence and activity in the Chummetjitälli. Red line = active rockglacier, yellow line = inactive rockglacier, green line = relict rockglacier. Given numbers correspond to the inventory table (table 5.4). Underlying orthophoto of 20.08.1975 (flight-line 22, aerial photographs taken by Swisstopo).
- Figure 5.10:** Vertical surface changes in the Chummetjitälli between 1975 and 2001 (DTM comparison).
- Figure 5.11:** Rockglacier occurrence and activity in the Brändjitälli. Red line = active rockglacier. Given numbers correspond to the inventory table (table 5.5). Underlying orthophoto of 20.08.1975 (flight-line 22, aerial photographs taken by Swisstopo).
- Figure 5.12:** Vertical surface changes in the Brändjitälli between 1975 and 2001 (DTM comparison).
- Figure 5.13:** Rockglacier occurrence and activity in the Pipjitälli. Red line = active rockglacier, yellow line = inactive rockglacier. Given numbers correspond to the inventory table (table 5.6). Underlying orthophoto of 20.08.1975 (flight line 22, aerial photographs taken by Swisstopo).
- Figure 5.14:** Vertical surface changes in the Pipjitälli between 1975 and 2001 (DTM comparison).
- Figure 5.15:** Mean annual surface velocities between 1975 and 1993 on the rockglaciers Pipp1 and Pipp2. Underlying orthoimage of 20.08.1975 (flight line 22, aerial photographs taken by Swisstopo).
- Figure 5.16:** Mean annual surface velocities between 1993 and 2001 on the rockglaciers Pipp1 and Pipp2. Underlying orthoimage of 20.08.1975 (flight line 22, aerial photographs taken by Swisstopo).
- Figure 5.17:** Cumulative vertical change on rockglacier Pipp1 between 1975 and 1993 (smoothed by a median-filter, window size 3x3). Underlying orthoimage of 20.08.1975 (flight line 22, aerial photographs taken by Swisstopo).
- Figure 5.18:** Cumulative vertical change on rockglacier Pipp1 between 1993 and 2001 (smoothed by a median-filter, window size 3x3). Underlying orthoimage of 20.08.1975 (flight line 22, aerial photographs taken by Swisstopo).
- Figure 5.19:** Mean annual surface velocities 1975 – 2001 on the rockglacier Pipp4. Underlying orthoimage of 20.08.1975 (flight line 22, aerial photographs taken by Swisstopo).
- Figure 5.20:** Mean annual surface velocities 1975 – 1993 on the rockglacier Pibw. Underlying orthoimage of 20.08.1975 (flight line 22, aerial photographs taken by Swisstopo).
- Figure 5.21:** Mean annual surface velocities 1993 – 2001 on the rockglacier Pibw. Underlying orthoimage of 20.08.1975 (flight line 22, aerial photographs taken by Swisstopo).
- Figure 5.22:** Cumulative vertical change on rockglacier Pibw between 1975 and 1993 (smoothed by a median-filter, window size 3x3). Underlying orthoimage of 20.08.1975 (flight line 22, aerial photographs taken by Swisstopo).
- Figure 5.23:** Cumulative vertical change on rockglacier Pibw between 1993 and 2001 (smoothed by a median-filter, window size 3x3). Underlying orthoimage of 20.08.1975 (flight line 22, aerial photographs taken by Swisstopo).
- Figure 5.24:** Mean annual surface velocities 1975 – 1993 on the rockglacier Brho1. Underlying orthoimage of 20.08.1975 (flight line 22, aerial photographs taken by Swisstopo).
- Figure 5.25:** Mean annual surface velocities 1993 – 2001 on the rockglacier Brho1. Underlying orthoimage of 20.08.1975 (flight line 22, aerial photographs taken by Swisstopo).
- Figure 5.26:** Cumulative vertical change on the rockglaciers Brho1 and Brle between 1975 and 1993 (smoothed by a median-filter, window size 3x3). Underlying orthoimage of 20.08.1975 (flight line 22, aerial photographs taken by Swisstopo).

- Figure 5.27:** Cumulative vertical change on the rockglaciers Brho1 and Brle between 1993 and 2001 (smoothed by a median-filter, window size 3x3). Underlying orthoimage of 20.08.1975 (flight line 22, aerial photographs taken by Swisstopo).
- Figure 5.28:** Mean annual surface velocities 1975 – 1993 on the rockglacier Brle. Underlying orthoimage of 20.08.1975 (flight line 22, aerial photographs taken by Swisstopo).
- Figure 5.29:** Mean annual surface velocities 1993 – 2001 on the rockglacier Brle. Underlying orthoimage of 20.08.1975 (flight line 22, aerial photographs taken by Swisstopo).
- Figure 5.30:** Mean annual surface velocities 1975 – 1993 on the rockglacier Hufh. Underlying orthoimage of 20.08.1975 (flight line 22, aerial photographs taken by Swisstopo).
- Figure 5.31:** Mean annual surface velocities 1993 – 2001 on the rockglacier Hufh. Underlying orthoimage of 20.08.1975 (flight line 22, aerial photographs taken by Swisstopo).
- Figure 5.32:** Cumulative vertical change on rockglacier Hufh between 1975 and 1993 (smoothed by a median-filter, window size 3x3). Underlying orthoimage of 20.08.1975 (flight line 22, aerial photographs taken by Swisstopo).
- Figure 5.33:** Cumulative vertical change on rockglacier Hufh between 1993 and 2001 (smoothed by a median-filter, window size 3x3). Underlying orthoimage of 20.08.1975 (flight line 22, aerial photographs taken by Swisstopo).
- Figure 5.34:** Mean annual surface velocities 1975 – 1993 on the rockglacier Hujp. Underlying orthoimage of 20.08.1975 (flight line 22, aerial photographs taken by Swisstopo).
- Figure 5.35:** Mean annual surface velocities 1993 – 2001 on the rockglacier Hujp. Underlying orthoimage of 20.08.1975 (flight line 22, aerial photographs taken by Swisstopo).
- Figure 5.36:** Cumulative vertical change on rockglacier Hujp between 1975 and 1993 (smoothed by a median-filter, window size 3x3). Underlying orthoimage of 20.08.1975 (flight line 22, aerial photographs taken by Swisstopo).
- Figure 5.37:** Cumulative vertical change on rockglacier Hujp between 1993 and 2001 (smoothed by a median-filter, window size 3x3). Underlying orthoimage of 20.08.1975 (flight line 22, aerial photographs taken by Swisstopo).
- Figure 5.38:** Mean annual surface velocities 1975 – 1993 on the rockglacier Huhh1. Underlying orthoimage of 20.08.1975 (flight line 22, aerial photographs taken by Swisstopo).
- Figure 5.39:** Mean annual surface velocities 1993 – 2001 on the rockglacier Huhh1. Underlying orthoimage of 20.08.1975 (flight line 22, aerial photographs taken by Swisstopo).
- Figure 5.40:** Cumulative vertical change on rockglacier Huhh1 between 1975 and 1993 (smoothed by a median-filter, window size 3x3). Underlying orthoimage of 20.08.1975 (flight line 22, aerial photographs taken by Swisstopo).
- Figure 5.41:** Cumulative vertical change on rockglacier Huhh1 between 1993 and 2001 (smoothed by a median-filter, window size 3x3). Underlying orthoimage of 20.08.1975 (flight line 22, aerial photographs taken by Swisstopo).
- Figure 5.42:** Mean annual surface velocities 1975 – 1993 on the rockglacier Huhh2. Underlying orthoimage of 20.08.1975 (flight line 22, aerial photographs taken by Swisstopo).
- Figure 5.43:** Mean annual surface velocities 1993 – 2001 on the rockglacier Huhh2. Underlying orthoimage of 20.08.1975 (flight line 22, aerial photographs taken by Swisstopo).
- Figure 5.44:** Cumulative vertical change on rockglacier Huhh2 between 1975 and 1993 (smoothed by a median-filter, window size 3x3). Underlying orthoimage of 20.08.1975 (flight line 22, aerial photographs taken by Swisstopo).
- Figure 5.45:** Cumulative vertical change on rockglacier Huhh2 between 1993 and 2001 (smoothed by a median-filter, window size 3x3). Underlying orthoimage of 20.08.1975 (flight line 22, aerial photographs taken by Swisstopo).

- Figure 5.46:** Mean annual surface velocities 1975 – 1993 on the rockglacier Huhh3. Underlying orthoimage of 20.08.1975 (flight line 22, aerial photographs taken by Swisstopo).
- Figure 5.47:** Mean annual surface velocities 1993 – 2001 on the rockglacier Huhh3. Underlying orthoimage of 20.08.1975 (flight line 22, aerial photographs taken by Swisstopo).
- Figure 5.48:** Cumulative vertical change on rockglacier Huhh3 between 1975 and 1993 (smoothed by a median-filter, window size 3x3). Underlying orthoimage of 20.08.1975 (flight line 22, aerial photographs taken by Swisstopo).
- Figure 5.49:** Cumulative vertical change on rockglacier Huhh3 between 1993 and 2001 (smoothed by a median-filter, window size 3x3). Underlying orthoimage of 20.08.1975 (flight line 22, aerial photographs taken by Swisstopo).
- Figure 5.50:** Change in surface geometry of rockglacier Grueo1. Underlying orthoimages of 20.08.1975, 20.08.1993 (aerial photographs taken by Swisstopo) and 28.09.2001 (HRSC-A survey).
- Figure 5.51:** Mean annual surface velocities 1975 – 1981 on the rockglacier Grueo1. Underlying orthoimage of 20.08.1975 (flight line 22, aerial photographs taken by Swisstopo).
- Figure 5.52:** Mean annual surface velocities 1981 – 1987 on the rockglacier Grueo1. Underlying orthoimage of 16.08.1987 (flight line 34, aerial photographs taken by Swisstopo).
- Figure 5.53:** Mean annual surface velocities 1987 – 1993 on the rockglacier Grueo1. Underlying orthoimage of 20.08.1993 (flight line 16, aerial photographs taken by Swisstopo).
- Figure 5.54:** Mean annual surface velocities 1993 – 2001 on the rockglacier Grueo1. Underlying orthoimage of 28.09.2001 (HRSC-A data).
- Figure 5.55:** Cumulative vertical change on rockglacier Grueo1 between 1975 and 1981 (smoothed by a median-filter, window size 3x3). Underlying orthoimage of 20.08.1975 (flight line 22, aerial photographs taken by Swisstopo).
- Figure 5.56:** Cumulative vertical change on rockglacier Grueo1 between 1981 and 1987 (smoothed by a median-filter, window size 3x3). Underlying orthoimage of 20.08.1975 (flight line 22, aerial photographs taken by Swisstopo).
- Figure 5.57:** Cumulative vertical change on rockglacier Grueo1 between 1987 and 1993 (smoothed by a median-filter, window size 3x3). Underlying orthoimage of 20.08.1975 (flight line 22, aerial photographs taken by Swisstopo).
- Figure 5.58:** Cumulative vertical change on rockglacier Grueo1 between 1993 and 2001 (smoothed by a median-filter, window size 3x3). Underlying orthoimage of 20.08.1975 (flight line 22, aerial photographs taken by Swisstopo).
- Figure 5.59:** Mean annual surface velocities 1975 – 1993 on the rockglacier Grueo2. Underlying orthoimage of 20.08.1975 (flight line 22, aerial photographs taken by Swisstopo).
- Figure 5.60:** Mean annual surface velocities 1993 – 2001 on the rockglacier Grueo2. Underlying orthoimage of 20.08.1975 (flight line 22, aerial photographs taken by Swisstopo).
- Figure 5.61:** Cumulative vertical change on rockglacier Grueo2 between 1975 and 1993 (smoothed by a median-filter, window size 3x3). Underlying orthoimage of 20.08.1975 (flight line 22, aerial photographs taken by Swisstopo).
- Figure 5.62:** Cumulative vertical change on rockglacier Grueo2 between 1993 and 2001 (smoothed by a median-filter, window size 3x3). Underlying orthoimage of 20.08.1975 (flight line 22, aerial photographs taken by Swisstopo).
- Figure 5.63:** Mean annual surface velocities 1975 – 1993 on the rockglacier Grueo3. Underlying orthoimage of 20.08.1975 (flight line 22, aerial photographs taken by Swisstopo).
- Figure 5.64:** Mean annual surface velocities 1993 – 2001 on the rockglacier Grueo3. Underlying orthoimage of 20.08.1975 (flight line 22, aerial photographs taken by Swisstopo).

- Figure 5.65:** Cumulative vertical change on rockglacier Grueo3 between 1975 and 1993 (smoothed by a median-filter, window size 3x3). Underlying orthoimage of 20.08.1975 (flight line 22, aerial photographs taken by Swisstopo).
- Figure 5.66:** Cumulative vertical change on rockglacier Grueo3 between 1993 and 2001 (smoothed by a median-filter, window size 3x3). Underlying orthoimage of 20.08.1975 (flight line 22, aerial photographs taken by Swisstopo).
- Figure 5.67:** Mean annual surface velocities 1975 – 1993 on the rockglacier Grueo4. Underlying orthoimage of 20.08.1975 (flight line 22, aerial photographs taken by Swisstopo).
- Figure 5.68:** Mean annual surface velocities 1993 – 2001 on the rockglacier Grueo4. Underlying orthoimage of 20.08.1975 (flight line 22, aerial photographs taken by Swisstopo).
- Figure 5.69:** Cumulative vertical change on rockglacier Grueo4 between 1975 and 1993 (smoothed by a median-filter, window size 3x3). Underlying orthoimage of 20.08.1975 (flight line 22, aerial photographs taken by Swisstopo).
- Figure 5.70:** Cumulative vertical change on rockglacier Grueo4 between 1993 and 2001 (smoothed by a median-filter, window size 3x3). Underlying orthoimage of 20.08.1975 (flight line 22, aerial photographs taken by Swisstopo).
- Figure 5.71:** Mean annual surface velocities 1975 – 1993 on the rockglacier Grueo6. Underlying orthoimage of 06.10.1975 (flight line 21, aerial photographs taken by Swisstopo).
- Figure 5.72:** Mean annual surface velocities 1993 – 2001 on the rockglacier Grueo6. Underlying orthoimage of 06.10.1975 (flight line 21, aerial photographs taken by Swisstopo).
- Figure 5.73:** Cumulative vertical change on rockglacier Grueo6 between 1975 and 1993 (smoothed by a median-filter, window size 3x3). Underlying orthoimage of 06.10.1975 (flight line 21, aerial photographs taken by Swisstopo).
- Figure 5.74:** Cumulative vertical change on rockglacier Grueo6 between 1993 and 2001 (smoothed by a median-filter, window size 3x3). Underlying orthoimage of 06.10.1975 (flight line 21, aerial photographs taken by Swisstopo).
- Figure 5.75:** Mean annual surface velocities 1975 – 1993 on the rockglacier Grueo7. Underlying orthoimage of 06.10.1975 (flight line 21, aerial photographs taken by Swisstopo).
- Figure 5.76:** Mean annual surface velocities 1993 – 2001 on the rockglacier Grueo7. Underlying orthoimage of 06.10.1975 (flight line 21, aerial photographs taken by Swisstopo).
- Figure 5.77:** Cumulative vertical change on rockglacier Grueo7 between 1975 and 1993 (smoothed by a median-filter, window size 3x3). Underlying orthoimage of 06.10.1975 (flight line 21, aerial photographs taken by Swisstopo).
- Figure 5.78:** Cumulative vertical change on rockglacier Grueo7 between 1993 and 2001 (smoothed by a median-filter, window size 3x3). Underlying orthoimage of 06.10.1975 (flight line 21, aerial photographs taken by Swisstopo).
- Figure 5.79:** Mean annual surface velocities 1975 – 1993 on the rockglacier Niggel1. Underlying orthoimage of 20.08.1975 (flight line 22, aerial photographs taken by Swisstopo).
- Figure 5.80:** Mean annual surface velocities 1993 – 2001 on the rockglacier Niggel1. Underlying orthoimage of 20.08.1975 (flight line 22, aerial photographs taken by Swisstopo).
- Figure 5.81:** Cumulative vertical change on rockglacier Niggel1 between 1975 and 1993 (smoothed by a median-filter, window size 3x3). Underlying orthoimage of 20.08.1975 (flight line 22, aerial photographs taken by Swisstopo).
- Figure 5.82:** Cumulative vertical change on rockglacier Niggel1 between 1993 and 2001 (smoothed by a median-filter, window size 3x3). Underlying orthoimage of 20.08.1975 (flight line 22, aerial photographs taken by Swisstopo).
- Figure 5.83:** Mean annual surface velocities 1975 – 1993 on the rockglacier Niggel2. Underlying orthoimage of 20.08.1975 (flight line 22, aerial photographs taken by Swisstopo).

- Figure 5.84:** Mean annual surface velocities 1993 – 2001 on the rockglacier Niggel2. Underlying orthoimage of 20.08.1975 (flight line 22, aerial photographs taken by Swisstopo).
- Figure 5.85:** Cumulative vertical change on rockglacier Niggel2 between 1975 and 1993 (smoothed by a median-filter, window size 3x3). Underlying orthoimage of 20.08.1975 (flight line 22, aerial photographs taken by Swisstopo).
- Figure 5.86:** Cumulative vertical change on rockglacier Niggel2 between 1993 and 2001 (smoothed by a median-filter, window size 3x3). Underlying orthoimage of 20.08.1975 (flight line 22, aerial photographs taken by Swisstopo).
- Figure 5.87:** Mean annual surface velocities 1975 – 1993 on the rockglacier Chummet1. Underlying orthoimage of 20.08.1975 (flight line 22, aerial photographs taken by Swisstopo).
- Figure 5.88:** Mean annual surface velocities 1993 – 2001 on the rockglacier Chummet1. Underlying orthoimage of 20.08.1975 (flight line 22, aerial photographs taken by Swisstopo).
- Figure 5.89:** Cumulative vertical change on rockglacier Chummet1 between 1975 and 1993 (smoothed by a median-filter, window size 3x3). Underlying orthoimage of 20.08.1975 (flight line 22, aerial photographs taken by Swisstopo).
- Figure 5.90:** Cumulative vertical change on rockglacier Chummet1 between 1993 and 2001 (smoothed by a median-filter, window size 3x3). Underlying orthoimage of 20.08.1975 (flight line 22, aerial photographs taken by Swisstopo).
- Figure 5.91:** Comparison of mean annual horizontal velocities (m/a) between 1975-1993 and 1993-2001.
- Figure 5.92:** Comparison of median values of annual horizontal velocities (m/a) between 1975-1993 and 1993-2001.
- Figure 5.93:** Comparison of maximum annual horizontal velocities (m/a) between 1975-1993 and 1993-2001.
- Figure 5.94:** Horizontal surface velocity (m) of blocks on rockglacier Huhh1 between 10.9.2001 and 30.8.2002. Underlying orthophoto of 20.08.1975 (flight-line 22, aerial photographs taken by swisstopo).
- Figure 5.95:** Vertical change (m) of blocks on rockglacier Huhh1 between 10.9.2001 and 30.8.2002. Underlying orthophoto of 20.08.1975 (flight-line 22, aerial photographs taken by swisstopo).
- Figure 5.96:** Horizontal surface velocity (m) of blocks on rockglacier Huhh1 between 30.8.2002 and 10.8.2003. Underlying orthophoto of 20.08.1975 (flight-line 22, aerial photographs taken by swisstopo).
- Figure 5.97:** Vertical change (m) of blocks on rockglacier Huhh1 between 30.8.2002 and 10.8.2003. Underlying orthophoto of 20.08.1975 (flight-line 22, aerial photographs taken by swisstopo).
- Figure 5.98:** Horizontal surface velocity (m) of blocks on rockglacier Huhh1 between 10.8.2003 and 31.7.2004. Underlying orthophoto of 20.08.1975 (flight-line 22, aerial photographs taken by swisstopo).
- Figure 5.99:** Vertical change (m) of blocks on rockglacier Huhh1 between 10.8.2003 and 31.7.2004. Underlying orthophoto of 20.08.1975 (flight-line 22, aerial photographs taken by swisstopo).
- Figure 5.100:** Horizontal surface velocity (m) on rockglacier Huhh3 between 2.9.2002 and 13.8.2003. Underlying orthophoto of 20.08.1975 (flight-line 22, aerial photographs taken by swisstopo).
- Figure 5.101:** Horizontal surface velocity (m) on rockglacier Huhh3 between 13.8.2003 and 1.8.2004. Underlying orthophoto of 20.08.1975 (flight-line 22, aerial photographs taken by swisstopo).

- Figure 5.102:** Vertical change (m) on rockglacier Huhh3 between 2.9.2002 and 13.8.2003. Underlying orthophoto of 20.08.1975 (flight-line 22, aerial photographs taken by swisstopo).
- Figure 5.103:** Vertical change (m) on rockglacier Huhh3 between 13.8.2003 and 1.8.2004. Underlying orthophoto of 20.08.1975 (flight-line 22, aerial photographs taken by swisstopo).
- Figure 5.104:** Horizontal surface velocity (m) on rockglacier Huhh3 between 8.7. and 13.8.2003. Underlying orthophoto of 20.08.1975 (flight-line 22, aerial photographs taken by swisstopo).
- Figure 5.105:** Vertical change (m) on rockglacier Huhh3 between 8.7. and 13.8.2003. Underlying orthophoto of 20.08.1975 (flight-line 22, aerial photographs taken by swisstopo).
- Figure 5.106:** Compression wood in *Pinus cembra* stem and inferred movement of the ground.
- Figure 5.107:** Micro sections of *Salix helvetica* roots from an inactive rockglacier (Ref) (A) and an active rockglacier (BG) (B); Black arrows indicate vessels (magnification: 40x). The differences in size of the vessels of unstressed (A) and stressed (B) roots are remarkable.
- Figure 5.108:** Boxplot visualisation of vessel size data (compare table 5.15): (A) active; (B) inactive rockglacier; (C) average values of vessel sizes (A) and (B). The skewed distribution is due to the exclusion of all cells $< 0.0002 \text{ mm}^2$ (tracheids), the scale was adjusted to a max. value of 0.004 mm^2 for better visualisation.
- Figure 5.109:** Bottom Temperatures of the winter Snow cover (BTS) on rockglacier Huhh1 in three successive years. Underlying orthophoto of 20.08.1975 (flight-line 22, aerial photographs taken by swisstopo).
- Figure 5.110:** Bottom Temperatures of the winter Snow cover (BTS) on rockglacier Huhh3 in three successive years. Underlying orthophoto of 20.08.1975 (flight-line 22, aerial photographs taken by swisstopo).
- Figure 5.111:** Bottom Temperatures of the winter Snow cover (BTS) on the inactive rockglacier Hurh2 in three successive years. Underlying orthophoto of 20.08.1975 (flight-line 22, aerial photographs taken by swisstopo).
- Figure 5.112:** Bottom Temperatures of the winter Snow cover (BTS) on the inactive rockglacier Huhh2 in three successive years. Underlying orthophoto of 20.08.1975 (flight-line 22, aerial photographs taken by swisstopo).

CHAPTER 6

- Figure 6.1:** Relation between average slope ($^{\circ}$) and mean annual horizontal velocity (m/a) of all active rockglaciers (apart from Grueo1) for both investigated periods. \square = mean velocity 1975 – 1993; $\bar{\Delta}$ = mean velocity 1993 – 2001. Total sample size $n = 16$. Thus, $r^*_{95} = 0.497$, $r^*_{99} = 0.623$, $r^*_{99.9} = 0.742$.
- Figure 6.2:** Relation between rockglacier length (m) and mean annual horizontal velocity (m/a) of all active rockglaciers (apart from Grueo1) for both investigated periods. \square = mean velocity 1975 – 1993; $\bar{\Delta}$ = mean velocity 1993 – 2001. Total sample size $n = 16$.
- Figure 6.3:** Relation between altitude of rockglacier front (m a.s.l.) and mean annual horizontal velocity (m/a) of all active rockglaciers (apart from Grueo1) for both investigated periods. \square = mean velocity 1975 – 1993; $\bar{\Delta}$ = mean velocity 1993 – 2001; \square = Huhh3 mean velocity 1975 – 1993 (not included in the trendline – analysis); \square = Huhh3 mean velocity 1993 – 2001 (not included in the trendline-analysis).
- Figure 6.4:** Relation between MAAT ($^{\circ}\text{C}$) at rockglacier front and mean annual horizontal velocity (m/a) of all active rockglaciers (apart from Grueo1) for both investigated periods. \square = mean velocity 1975 – 1993; $\bar{\Delta}$ = mean velocity 1993 – 2001; \square = Huhh3 mean velocity 1975 – 1993 (not included in the trendline – analysis); \square = Huhh3 mean velocity 1993 – 2001 (not included in the trendline-analysis).

Figure 6.5: Mean annual air temperatures (black line), mean summer air temperatures (upper grey line) and mean winter air temperatures (lower grey line) at the Sion station (482 m a.s.l.) between 1864 and 2002 (according to Böhm et al. 2001). The distance to the Turtmann valley is about 26 km. The depicted trendline demonstrates the positive trend of the temperature.

Figure 6.6: Comparison of flow fields (A) and BTS-temperatures (B) on rockglacier Huhh1 (front orientation to the north). A: Mean annual horizontal velocity (m/a) of the period 1993-2001 measured by digital photogrammetry, summarised in several flow fields. B: BTS-values of the winters 2001/2002, 2002/2003 and 2003/2004 on rockglacier Huhh1 (from: Roer et al. in press).

Figure 6.7: Comparison of flow fields (A) and BTS-temperatures (B) on rockglacier Huhh3 (front orientation to the northwest). A: Mean annual horizontal velocity (m/a) of the period 1993 – 2001 measured by digital photogrammetry, summarised in several flow fields. B: BTS-values of the winters 2001/2002, 2002/2003 and 2003/2004 on rockglacier Huhh3.

LIST OF TABLES

CHAPTER 3

Table 3.1: Sensor parameters of aerial photography and HRSC-A data (modified, after Hoffmann 2000).

Table 3.2: Flight parameters and properties of aerial photography and HRSC-A data for the Turtmann valley.

Table 3.3: Technical details of the Leica tachymeter TCA 1800L (cf., Kahmen 1997).

CHAPTER 4

Table 4.1: Elevation, mean annual precipitation and mean annual air temperature for selected stations in the Rhone valley (1-7), the Matter valley (8-11), the Anniviers valley (12, 13) and the Hérens valley (14, 15). Apart from station Evolène, the SMA-values represent mean values of the period 1901 – 1960.

CHAPTER 5

Table 5.1: Rockglacier inventory of the Hungerlitälli.

Table 5.2: Rockglacier inventory of the Grübttälli.

Table 5.3: Rockglacier inventory of the Niggelintälli.

Table 5.4: Rockglacier inventory of the Chummetjtälli.

Table 5.5: Rockglacier inventory of the Brändjtälli.

Table 5.6: Rockglacier inventory of the Pipjtälli.

Table 5.7: Comparison of horizontal velocities (mean, median, maximum) between 1975-1993 and 1993-2001 of all investigated active rockglaciers.

Table 5.8: Comparison of horizontal velocities (mean, median, maximum) of rockglacier Grueo1 over four investigated periods.

Table 5.9: Velocities of blocks at the surface of rockglacier HuHH1 in the period 2001/2002 and 2002/2003.

Table 5.10: Velocities of blocks at the surface of rockglacier HuHH1 in the period 2003/2004 and between July and August of 2003.

Table 5.11: Measured velocities of blocks at the surface of rockglacier HuHH1 for the entire period 2001/2004 (only for the blocks measured in 2001) and addition of the single periods (as check).

Table 5.12: Velocities of blocks at the surface of rockglacier Huhh3 between 2002-2003 and 2003-2004.

Table 5.13: Velocities of blocks on Huhh3 over the whole period 2002-2004 and for comparison check of horizontal and vertical changes by addition of the values 2002-2003 (t1) and 2003-2004 (t2).

Table 5.14: Direction, horizontal and vertical change of blocks on Huhh3 between 8.07. and 13.08.2003 as well as contribution to the 'annual' displacement (2.9.2002 – 13.8.2003) in percent.

Table 5.15: Median, maximum, minimum values of vessel sizes and their statistical spread (*Salix helvetica* roots); inactive (Ref) and active (BG) rockglacier.

ACRONYMS

a.s.l.	above sea level
ATR	Automatic Target Recognition system
BTS	Bottom Temperature of the winter Snow cover
CCD	Charge Coupled Devices
CIAS	Correlation Image Analysis
DInSAR	Differential Interferometric Synthetic Aperture Radar
DLR	Deutsches Zentrum für Luft- und Raumfahrt / German Aerospace Center
DTM	Digital Terrain Model
EDM	Electronic Distance Meter
GCP	Ground Control Point
GIS	Geographical Information System
GPS	Global Positioning System
HRSC-A	High Resolution Stereo Camera – Airborne
IDL	Interactive Data Language
INS	Inertial Navigation System
LIA	Little Ice Age
MAAT	Mean Annual Air Temperature
MAGST	Mean Annual Ground Surface Temperature
RMS	Root Mean Square error
SMA	Schweizer Meteorologische Anstalt
UTL	Universal Temperature Logger

1 INTRODUCTION

Geomorphology will achieve its fullest development only when the forms and processes are related in terms of dynamic systems and the transformations of mass and energy are considered as functions of time. (Strahler 1952: 935)

This quotation unites in one sentence both foundation and objective of the current geomorphological research. It gives a clear definition of ‘geomorphology’ within the context of the systems approach building the conceptual and methodological basis. In addition to that it aims at the heart of the here presented study: the analysis of dynamic systems by determination of mass and energy fluxes. Regarding the focus of this study, the high mountain geosystem which is characterised by an extensive transfer of mass and energy, it is also well reflected in this statement.

1.1 Motivation

The increasing interest in recent climatic change and its impact on geosystems confirms the significance of high-mountain environments as sensitive key areas, and not only since the events during the hot summer of 2003. Global environmental change is the result of interactions and feedbacks among the earth’s different subsystems at a wide range of spatial and temporal scales. General circulation models predict the major temperature changes in high latitudes (polar region) and high altitudes (high mountains) since horizontal and vertical gradients of the atmospheric variables are more extensive and thus small changes in environmental conditions are noted earlier (Slaymaker & Spencer 1998). This is confirmed for example by a temperature increase, which occurred more intensely in the Alps than elsewhere (e.g., Böhm 2003).

Within the high mountain system, landforms (e.g., glaciers) or ecological boundaries (e.g., lower boundary of permafrost occurrence, tree line) are monitored systematically and act as important indicators for environmental changes (e.g., IPCC 2001a, b). While the sensitivity of periglacial landscapes (in high latitudes as well as in high altitudes) was often considered (e.g., Lachenbruch & Marshall 1986; Anisimov & Nelson 1996), the indicative role of rockglaciers in this context was emphasised only recently (e.g., Harris & Haeberli 2003).

1.2 Objectives

In the 80-year history of rockglacier research, movements were often described and quantified (see appendix 1), but the processes behind and thus the dynamics of the permafrost bodies are still not known in detail. Apart from the measurements at the rockglacier surface (e.g., Kääb et al. 2003), borehole studies (e.g., Hoelzle et al. 1998; Arenson et al. 2002) and laboratory tests (e.g.,

Davies et al. 2001) improved the knowledge during the last decade. But, these investigations are often concentrated on single rockglaciers, due to methodological and financial limitations.

For further investigations of rockglacier creep, several research needs and objectives arise:

- High accuracy techniques and data with high spatial and temporal resolution are required for the quantification of rockglacier movement.
- Long monitoring series on rockglacier kinematics are demanded on large spatial scales (several neighbouring rockglaciers) to analyse spatio-temporal variations reliably.
- In order to deepen the knowledge on rockglacier dynamics, influencing parameters (e.g., temperature, snow cover characteristics, debris supply, etc.) need to be included in the analysis of spatial and temporal variations.
- The sensitivity of rockglaciers has to be determined in order to use these landforms as indicators for changing environmental conditions in high mountain geosystems

The high density of rockglaciers in the Turtmann valley (Swiss Alps) and the existing data on their characteristics and distribution (Nyenhuis 2001; Roer 2001) suggested the area-wide quantification of rockglacier creep for the characterisation of this high mountain geosystem. Some data on rockglacier movements already existed for the study site (Elverfeldt 2002), but they were not sufficient for the analysis of spatial and temporal variations. Therefore, rockglacier kinematics, which is defined as the quantification of movement without considering the forcing factors (in contrast to dynamics), is investigated by the application of different methods.

From the given objectives and in view of the current state of the art (cf., chapter 2), the following research questions are compiled for the here presented study:

- Are the applied methods and the available data suited to the quantification of rockglacier creep in high mountain environments? Which advantages, limitations, resolutions and accuracies are revealed by the different methods?
- Do the applied techniques allow the reliable assessment of the state of activity?
- What are the mean and maximum values of horizontal as well as vertical displacements; also in comparison to other rockglaciers in the Alps?
- Do the movements reflect spatio-temporal variations? Is it possible to distinguish seasonal and interannual variations from longterm trends?
- To what extent are the horizontal velocities and vertical changes conditional upon terrain parameters or climatic influences?
- Is it possible to assess the sensitivity of rockglaciers and thus evaluate their geomorphic and environmental significance in the high mountain geosystem?

1.3 Conceptual background

As part of the Research Training Group 'Landform – a structured and variable boundary layer' (Graduierkolleg 437) the focus of the study is given on landforms, their characteristics and spatial distribution as well as their changes in time. In general, landform is characterised by

certain structures or patterns, since it is not distributed arbitrarily in space. Penck (1894) was the first who designed a hierarchy of landforms which was later modified by Kugler (1974) who introduced the term ‘complexity’ in this context and by Büdel (1977) who considered nested hierarchies. For a review of these classical concepts in geomorphology as well as the parameterization of landform, it is referred to Rasemann (2004).

In the study presented here, landform is considered as a boundary layer or interface, respectively, between the atmosphere/hydrosphere/cryosphere and the pedosphere/lithosphere and thus represents both control factor and result (form, shape) of processes, acting on different spatial and temporal scales. The boundary layer or landform is regarded as a 2-dimensional object in the 4-dimensional space with certain geometrical characteristics, which can be considered in a geomorphodynamic context (Dikau & Schmidt 1999). Here, focus is given on one specific landform (rockglacier), its distribution in space, its activity, its temporal changes in geometry as well as the probable reasons for its change. The repeated measurement of the object geometry allows the quantification of corresponding process rates. Thus, the temporal scale is explicitly included. By consulting the model of the boundary condition (cf., chapter 2.3.5.4) a quasi - 4D-consideration of the rockglaciers is enabled.

Related to the phenomena such as permafrost and rockglacier creep, landform is of significance on various scales. Permafrost is a thermally controlled phenomenon, which can be considered on macro or meso-scale with parameters like mean annual air temperature (MAAT) or solar radiation. But on the micro-scale, different parameters such as latent heat fluxes, snowcover or properties of the substratum are of major importance (cf., chapter 2.2.2). Thus, the scale of consideration influences the determination of relevant parameters decisively. The interconnexion of different scales can be resolved by upscaling- and downscaling techniques. This multiscale approach is based on the consideration of systems in a hierarchical configuration: a system is part of a larger system and can itself be composed of several smaller systems. The systems theory found application in geomorphology by the contributions of Strahler (1952), Hack (1960) and Chorley (1962) and developed into a unifying concept in physical geography by the book: *Physical geography: a systems approach* (Chorley & Kennedy 1971).

Regarding the four system types stated by Chorley & Kennedy (1971) the here presented study depicts a **simple process-response system**, “*which is formed by the intersection of morphological and cascading systems and involving emphasis upon processes and the resulting forms*” (Gregory 2000: 88). This is based on an empirical as well as on a conceptual dynamic model. It is part of the more comprehensive cascading system which is considered in the Turtmann valley to describe the sediment budget of a high mountain geosystem (Nyenhuis 2005).

Different scales are considered in this study, depending on the relevant scale of the phenomenon and the available data. According to the classification by Dikau (1989), the landform ‘rockglacier’ analysed in this study belongs to the microrelief and is thus regarded on the micro-scale (Figure 1.1). But, due to the applied techniques, the rockglacier kinematics is quantified by the repeated measurement of single blocks at the rockglacier surface. Therefore, the data scale is established in the **nanorelief-level**, whereas results and conclusions are aggregated and compiled on a **micro-**

to mesorelief level (scale of phenomenon). Regarding the **temporal scale**, the data scale is restricted to a period of 29 years by the application of different methods with diverse resolutions. Against that, the scale of the phenomenon (permafrost creep) is referred to the entire Holocene, as the rockglaciers formed during that period and thus depict complex archives of climatic history. Since for rockglaciers reaction times to climatic changes are far from known, the interpretations refer to the last century including the warming after the little ice age (LIA). Thus the temporal scale of the data and the one of the interpretation are not identical and therefore conclusions on relevant forcing factors are probably limited.

	Main type of size order			Type of size order			Examples	This study
	W (m)	A (m ²)	H/D (m)	W (m)	A (m ²)	H/D (m)		
MEGARELIEF	>10 ⁶	>10 ¹²		>10 ⁶	>10 ¹²		Canadian shield	
B MACRORELIEF	10 ⁶	10 ¹²	>10 ³	10 ⁶	10 ¹²	>10 ³	Mountain area, Alps, Rhine	
A MESORELIEF	10 ⁴	10 ⁸	10 ³	10 ⁴	10 ⁸	10 ³	Valley, moraine, hills	Valley Hanging valley
B MICRORELIEF	10 ²	10 ⁴	10 ¹	10 ²	10 ⁴	10 ¹	Gully, dune, terrace	Rockglacier
A NANORELIEF	10 ⁰	10 ⁰	10 ⁻¹	10 ⁰	10 ⁰	10 ⁻¹	Erosion rills	Block on rockglacier surface
PICORELIEF	10 ⁻²	10 ⁻⁴	<10 ⁻¹	10 ⁻²	10 ⁻⁴	<10 ⁻¹	Glacial striations	

W = width of unit A = area of unit H/D = height/depth of unit

Figure 1.1: Hierarchical level and size of relief units (modified, after Dikau 1989). Bold face indicates relief units considered in this study.

The presented study outlines the scientific background of permafrost and rockglacier research in high mountain geosystems and focuses on the recent developments (**chapter 2**); it gives a thorough compilation of published data on rockglacier kinematics (**appendix 1**); it presents the advantages and limitations of the applied methods and the corresponding spatial and temporal resolution of the data (**chapter 3**); it introduces the study area (**chapter 4**); presents the results and interpretation of rockglacier kinematics (**chapter 5**); gives a discussion on the findings including rheological considerations (**chapter 6**) and ends with conclusions and perspectives (**chapter 7, 8**).

2 SCIENTIFIC BACKGROUND

2.1 High mountain geosystems

2.1.1 Definition & characteristics

The description of mountain environments had its beginning in the documentation by Alexander von Humboldt and Aimé Bonpland who described altitudinal belts in a cross-section of the Andes linking physical parameters with biological observations (Humboldt 1807; Messerli & Ives 1997). Later, most classifications applied single geomorphological parameters such as altitude or steepness of slope to describe high mountains in a quantitative way (Penck 1894; Passarge 1921). But, comparing mountains all over the world, the approaches were inadequate for a unifying definition. Thus, combinations of several parameters were suggested in order to represent high mountain characteristics; Rathjens (1982), Gerrard (1990), Bishop & Shroder (2004), as well as Owens & Slaymaker (2004) provide useful reviews of these classifications. Barsch & Caine (1984) proposed four criteria to determine mountain terrain:

- elevation,
- steep gradients,
- rocky terrain and
- the presence of snow and ice.

Additionally, they depicted a relative relief (i.e., the difference between the maximum elevation of a peak and the elevation of the surrounding terrain) of 500 m/km² as a criterion of high mountain systems (Barsch & Caine 1984: 288).

Parallel to these morphological approaches, Troll (1941, 1966, 1973) and Höllermann (1973) followed the geocological attempt of Humboldt and compiled a comprehensive description of high mountain nature. Troll studied various mountain ranges in order to find characteristics which are applicable all over the world. Finally, he described a high mountain ecosystem as one which extends above:

- the Pleistocene snowline (indicating the variety of glacial landforms),
- the lower boundary of recent periglacial dynamics (lower limit of solifluction, conditioned upon freeze and thaw cycles) and
- the upper timberline.

These 'lines' are more or less close to each other and build up a transition belt that marks the lower margin of the high mountain area. Following this concept, "*high-mountains are mountains which reach such altitudes that they offer landforms, plant cover, soil processes, and landscape character which in the classical region of mountain geography in the Alps is generally perceived as high-alpine*" (Troll 1972, in Höllermann 1973).

Based on this definition, Troll (1966, 1973) documented an additional subdivision of high mountains into three characteristic subbelts:

- a lower subbelt with a close plant cover and with hampered solifluction,
- a middle subbelt of debris cover with a scanty pioneer vegetation and free solifluction, and
- the nival belt above the climatic snow line.

Recently, more holistic descriptions of mountain environments are formulated, e.g. by Messerli & Ives (1997) who integrate and emphasise the role of human beings within this system: "*Mountains, obviously, are regions of accentuated relief and altitude, which influence climate, soil fertility, vegetation, slope instability, and accessibility.*".

As it is apparent from the literature, a rigorous and representative description of high mountains is hard to define, since morphological, climatic as well as biological parameters interact in a complex system and thus lead to a great variability in shape and structure of mountain geosystems. Hence, although this study is concentrated on landforms, the consideration of high mountain geosystems in a pure geomorphological context would be restrictive. Thus, the approach of Troll is emphasised in this investigation. Especially the second 'line' described by Troll directly refers to the purpose of this study; i.e., the measurement of rockglacier kinematics as part of the periglacial dynamics. These landforms are considered as significant indicators for changes at the lower limit of high mountain geosystems. In general, the sensitivity and thus the significance of these systems need to be considered. Regarding mountain geomorphology, Barsch & Caine (1984) stated that it deserves special attention within geomorphology, since due to criteria like steep gradients, environmental changes may occur on shorter time-scales and with lasting consequences. Thus, in spite of a great complexity and variability these changes need to be monitored and sensitivities as well as thresholds need to be identified. They are of great importance if geomorphology is to be useful in prediction.

2.1.2 High mountain geomorphology

High mountain geomorphology is characterised by steep rock walls ($> 60^\circ$) and steep slopes ($35-60^\circ$), forming a high-energy environment (Barsch & Caine 1984). Thus, a strong correlation exists between erosion rate and relief (Gerrard 1990). Low relief can only be found on mountain plateaus or on the floor of valleys, since they are filled with sediment of glacial, periglacial and fluvial processes.

In most high mountain areas the topography is dominated by glacial-genetic bedrock forms (nunataks, cirques, glacial troughs), as evidence of former (Pleistocene) glacial activity (**glacial erosion**). These macro- to mesorelief-forms are superimposed by meso- to microrelief-forms (moraines, solifluction-lobes, talus cones, fans), which are due to diverse process-domains (glacial, periglacial, gravitational) acting more recently (cf. Anderson & Burt 1981) (**postglacial accumulation**) (Figure 2.1). This apparent disparity between present landforms and

contemporary processes seems to be especially evident in high mountain areas (Barsch & Caine 1984).

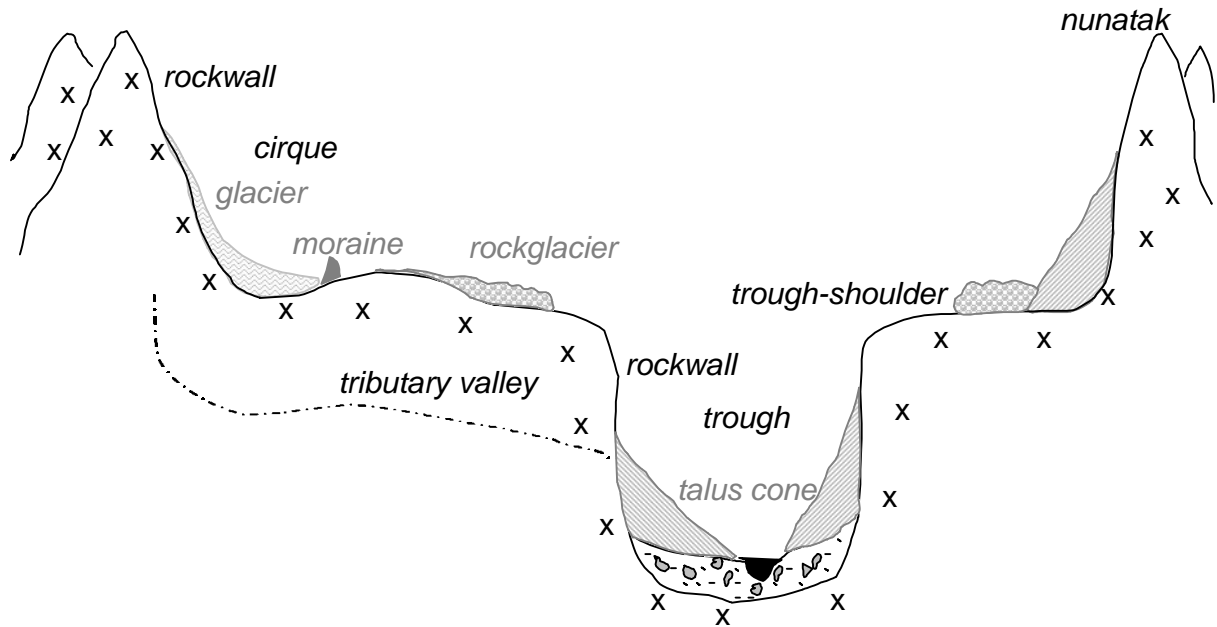


Figure 2.1: Some basic elements of high mountain landforms (modified, after Barsch & Caine 1984). Black lines and type: glacial erosive forms; grey lines and type: postglacial accumulative forms.

Another characteristic is the hypsometric sequence of typical landforms (Lautensach 1952). These are due to process domains (Thornes 1979) resulting from particular environmental parameters, e.g. slope, aspect, climatic conditions. Together with other phenomena such as vegetation, these sequences enable a subdivision in mountain belts: montane, subalpine, alpine, nival. The alpine belt, for example, is defined by the occurrence of solifluction (cf., Rathjens 1982). Concerning the processes operating and their significance as sediment transport systems, rate and intensity at which the processes operate need to be considered and discussed in the context of magnitude and frequency (Wolman & Miller 1960; Gerrard 1990).

2.2 Periglacial & Permafrost

2.2.1 Definition & characteristics

In general, the periglacial belt in mountains as well as in subpolar zones is characterised by freeze and thaw processes (cf., French 1996). Within high mountains it was defined by Troll (1973) as the area between the upper timberline and the snow line. Concerning a definition of the lower periglacial limit, the geomorphologic effectiveness of the cryogenic processes needs to be considered (cf., Hagedorn 1980). This was detailed by Troll, who subdivided the belt in two subbelts of different periglacial dynamics:

- “a lower subbelt beyond the timberline, where a close carpet of vegetation ... exists and where the frost action and the cryoturbation is hampered by and in competition with the growing plant cover...” (hampered or bound solifluction (cf., Büdel 1948; Höllermann 1985))
- “an upper substage ... with bare scree- and debris-soils and a very scanty pioneer vegetation ...” (free or unbound solifluction (cf., Höllermann 1985)).

In the Alps, a wide area above the timberline is influenced by the occurrence of permafrost, which is defined as lithospheric material with temperatures $< 0^{\circ}\text{C}$ during at least one year (e.g., Haeberli 1975). Thus, the phenomenon permafrost is closely related to the periglacial belt. But, as it is the same in subpolar regions, there is no obligatory overlap between periglacial and permafrost areas. The occurrence of permafrost is an indicator for periglacial conditions but it is not an essential attribute of the periglacial (Karte 1979; Thorn 1992).

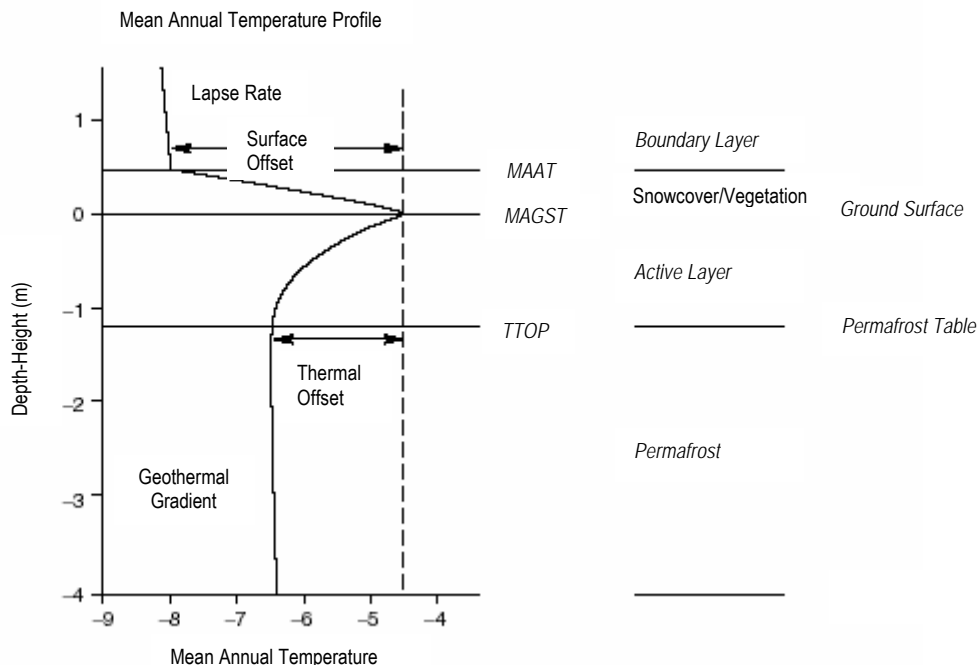


Figure 2.2: Schematic mean annual temperature profile through the surface boundary layer, showing the relation between air temperature and permafrost temperature (modified, after Smith & Riseborough 2002: 5). MAAT = Mean Annual Air Temperature; MAGST = Mean Annual Ground Surface Temperature; TTOP = mean annual Temperature at the Top Of Permafrost.

2.2.2 Influencing factors

As defined, the occurrence of permafrost is characterised by temperature and time and is primarily a function of direct solar radiation, air temperature, as well as the characteristics of soil, vegetation- and snowcover (Haeberli 1990). A typical temperature profile through the surface boundary layer of a permanently frozen ground is depicted in figure 2.2. In order to get a better understanding of the processes within, a lot of recent investigations deal with monitoring and modelling of vertical energy fluxes between permafrost body, active layer, ground surface and

atmosphere (e.g., Humlum 1998c; Stocker-Mittaz et al. 2002). The energy balance at the ground surface is expressed quantitatively in the following equation (Hoelzle et al. 1993; Hoelzle 1994):

$$Q_r \pm Q_h \pm Q_{lc} \pm Q_g \pm Q_m = 0$$

Where Q_r is the radiation balance, Q_h the sensible and Q_{lc} the latent heat flux, Q_g the conduction of heat into the ground and Q_m the heat of fusion of the ice (Hoelzle 1994). These components discussed in Hoelzle (1994) and Mittaz (1998) in more detail, are variable in space and time since they are influenced by climatic and topographic parameters (Hoelzle et al. 1993). Therefore, the permafrost occurrence is very complex - especially in high mountains, where the permafrost distribution varies strongly due to varying topography. Here, the radiation seems to be the dominating factor (e.g., Hoelzle 1992; Funk & Hoelzle 1992; Hoelzle 1994; Schrott 1994; Krummenacher et al. 1998). Additionally, also the thickness, redistribution and duration of the snowcover (e.g., Hoelzle 1992; Keller 1994; Krummenacher et al. 1998; Harris 2001; Mittaz et al. 2002; Hanson & Hoelzle 2004; Luetsch et al. 2004) as well as the characteristics of the surface material (Humlum 1998a; Herz et al. 2003; Hanson & Hoelzle 2004) play an important role. The knowledge on interrelationships of temperatures and permafrost occurrence on the local scale needs then to be applied to sophisticated models of permafrost distribution on a more regional scale (see below).

2.2.3 Prospecting methods

In order to get to know if permafrost is present in the ground or not, the best method is the direct measurement of temperatures in the ground (e.g., in boreholes) (e.g., Vonder Mühl 1993; Isaksen et al. 2001). Since this is a very expensive prospecting method, indirect means such as geophysical soundings (refraction seismics and DC-resistivity) are used for the determination of permafrost and its distribution (e.g., Dikau 1978; Haeberli & Epifani 1986; Barsch & King 1989; Vonder Mühl 1993; Vonder Mühl et al. 2001; Hauck 2001; Kneisel 2004). Additionally, in the seventies, the significance of the Bottom Temperature of the Snow cover (BTS) was detected as a reliable indicator for permafrost conditions (Haeberli 1973, 1975). Later, the development of miniature data loggers allowed longterm and continuous temperature measurements and improved the data dramatically (Hoelzle 1992; Hoelzle et al. 1993; Hoelzle et al. 1999; Imhof et al. 2000). Best interpretation is enabled by the combined application of different techniques.

2.2.4 Permafrost distribution, modelling & sensitivity

The permafrost distribution in the Alps is controlled by the spatial distribution of energy balance factors (see above) and is thus a function of topographic and climatic parameters (Hoelzle et al. 1993; Keller 1994). In view of these parameters and by considering the rules of thumb for permafrost distribution (Haeberli 1975) which build an important empirical basis, the probability of permafrost occurrence can be calculated using empirical-statistical or process-oriented models (Funk & Hoelzle 1992; Keller 1992; Hoelzle 1994; Imhof 1996; King 1996; Frauenfelder 1998; Gruber & Hoelzle 2001; Hoelzle et al. 2001; Stocker-Mittaz et al. 2002; Guglielmin et al. 2003). Concerning permafrost distribution models, the following spatial scales have been proposed

within the PACE project: a micro or patch scale with a spatial resolution of ≤ 25 m, a meso scale with a resolution of 25 to 200 m and a macro scale with a resolution > 250 m (Hoelzle et al. 2001: 55). Depending on the methodology applied and thus on the spatial and temporal scale considered, processes and the relative importance of influencing parameters are variable (e.g., De Boer 1992; Thorn 2003). E.g., on a local scale the permafrost distribution is influenced by snow distribution, vegetation cover, etc. while on a wider scale Mean Annual Air Temperature (MAAT) and solar radiation are consulted as the relevant factors. In this context, it is generally accepted that a MAAT of -2° C indicates discontinuous permafrost whereas a MAAT below -6° C shows continuous permafrost. In areas with mean annual air temperatures warmer than -2° C permafrost occurs only sporadically.

The increase in temperature within the last century has major consequences for the glacial and periglacial belt. The so far observed changes are mostly obvious reactions of the alpine environment on changing climate conditions (Haeberli 1992a, b; Haeberli 1995) and thus are important environmental indications. Additionally to the signal function, the resulting changes in mountain permafrost lead to problems in slope stability of rock and unconsolidated material (moraines, talus cones) (e.g., Haeberli et al. 1997; Nötzli et al. 2003). As a consequence, more data is demanded in order to deepen the knowledge on the ongoing processes and the reaction times of the system. Then, more sophisticated models can be developed to quantify mass fluxes and thus enable assessments on possible natural hazards (e.g., Käab & Haeberli 1996).

The 'system' permafrost reacts dynamically to environmental changes, whereas the reaction time of permafrost bodies is relevant for the understanding of the system (Haeberli 1990; Hoelzle 1994; Humlum 1998b; Frauenfelder & Käab 2000). Although the response of permafrost to climatic changes is not known in detail, one can consider that permafrost is very sensitive; even if it shows a delayed reaction to changes in the energy balance. The response time of permafrost depends primarily on the thickness of the permafrost body, the thermal conductivity, the ice content as well as on the amount of unfrozen water (e.g., Haeberli et al. 1993; Osterkamp 1983; Osterkamp & Romanovsky 1999). Direct and delayed reactions and adjustments can be distinguished, since direct response occurs at the permafrost table and results in the increasing thickness of the active layer. Against that, the delayed reaction affects the permafrost base and induces the thinning of the permafrost body. Concerning the relatively warm discontinuous permafrost in the Alps, a response time of several decades to centuries is assumed (cf., Haeberli 1990; Osterkamp & Romanovsky 1999). Haeberli (2000) stated that the permafrost thickness is presently not in equilibrium with the actual - in general warmer - ground surface temperatures. Thus it is assumed, that the actual permafrost occurrence reflects the climatic conditions of the Little Ice Age (LIA) (Etzelmüller & Hoelzle 2001).

The problems in permafrost research arise from the fact that the weighting of single factors (aspect, slope, snow cover, substrate, vegetation, etc.) and their significance within the energy balance is not sufficiently known. Therefore, actual permafrost studies concentrate on the filling of this gap. E.g., in order to get a better understanding of the relation between temperatures and the ground surface, the knowledge on rock temperatures, which show direct reactions since no

'buffer' layers (snow, vegetation, debris or talus) are present, is of major importance (Gruber et al. 2003; Gruber et al. 2004). Further improvements are claimed by the modelling of the former permafrost distribution (palaeopermafrost and palaeoclimate) (e.g., Frauenfelder & Kääb 2000) and possible developments in the future.

2.3 Rockglaciers

2.3.1 History of rockglacier research

In the beginning of the twentieth century so-called "*Rock Glaciers*" were described for the Rocky Mountains (Howe 1909) as well as for Alaska (Capps 1910) (from Pillewizer 1957). In Europe, Emil Chaix (1918; from Eugster 1973) was the first to call attention to these peculiar landforms he observed in the Swiss National Park. He started geomorphological investigations which were continued by André Chaix. By measuring stone lines on the rockglaciers Val Sassa and Val dell'Acqua, André Chaix (1923) delivered the first evidence on the movement of these features. Later, Heinrich Jäckli (1957) was concerned with the rockglaciers in this area. By 1920, in Austria E. de Martonne was the first to report on "*Blockgletscher*" in the Doisental (from Pillewizer 1957). In 1938, Pillewizer started investigations on rockglacier movement by means of terrestrial photogrammetry. The measurements were interrupted by the Second World War, but in the fifties he continued with detailed studies on the Hochebenkar rockglacier which until now provides the longest series on rockglacier movement (Pillewizer 1957; Vietoris 1972; Haeberli & Patzelt 1982). In recent times, rockglaciers are monitored in many places and by diverse methods (see Matsuoka & Humlum 2003 for summary).

2.3.2 Rockglacier origin & nomenclature

Since the second half of the twentieth century, rockglaciers were studied in diverse regions all over the world. At the same time, a wide discussion on the origin of these landforms started and two main positions evolved. One position focused on the glacial origin of rockglaciers (e.g., Outcalt & Benedict 1965; Potter 1972; Whalley 1974; Humlum 1982, 1988, 1996; Evans 1993; Whalley et al. 1994; Hamilton & Whalley 1995) while the others argued with a general periglacial origin (e.g., Wahrhaftig & Cox 1959; Haeberli 1985; Barsch 1977, 1988, 1992). Even some claim a polygenetic formation of rockglaciers as combination of periglacial, glacial and catastrophic mass movement processes (cf., Whalley & Martin 1992). Thus, rockglaciers may reflect geomorphic equifinality. Detailed discussions on rockglacier origin and nomenclature are given in several publications (e.g., Johnson 1983; Haeberli 1985; Corte 1987; Martin & Whalley 1987; Barsch 1987a, 1987b, 1992, 1996; Humlum 1988, 1996, 2000; Whalley & Martin 1992; Hamilton & Whalley 1995; Clark et al. 1998). The view that most rockglaciers are of periglacial origin has remained dominant since the comprehensive study on rockglaciers in Alaska by Wahrhaftig and Cox (1959).

The existing study follows the reasoning of Barsch and Haeberli. But, the influence of glaciers may not be denied in individual cases (see chapter 5.1.6). In general the terminology of the phenomenon (rockglacier) is a mistake, since the nomenclature implicitly relates to classical

glaciers. But, the latter belong to the hydrosphere, whereas rockglaciers with their debris-ice mixture are subordinated to the lithosphere. In order to emphasise the autonomy of the phenomenon, the term 'rockglacier' is written in one word according to Barsch (1988).

2.3.3 Rockglacier definition

Today, rockglaciers as well as ice-cored moraines are considered as morphological indicators for the presence of permafrost in high mountains (e.g., Haeberli 1985; Barsch 1996; Humlum 2000). In order to indicate the recent occurrence of permafrost, the considered rockglaciers need to be in an active status. Following Barsch (1992, p.176), "*active rockglaciers are lobate or tongue-shaped bodies of perennially frozen unconsolidated material supersaturated with interstitial ice and ice lenses that move downslope or downvalley by creep as a consequence of the deformation of ice contained in them and which are, thus, features of cohesive flow*". Haeberli (1985) focused on the process and described the phenomenon as "*visible expression of steady-state creep of ice-supersaturated mountain permafrost bodies in unconsolidated materials. They display the whole spectrum of forms created by cohesive flow*" (from Barsch 1992). The existing definitions give fundamental information on form, material and process, although the knowledge on the ongoing processes is still limited. A multiplicity of influencing parameters exists, but the interrelationships are often not known in detail.

2.3.4 Rockglacier distribution, morphology & stratigraphy

Detailed information on rockglacier occurrence, distribution and environmental conditions is given in Höllermann (1983), Haeberli (1985), Barsch (1992, 1996), and Humlum 2000. Large scale climatological boundary conditions can be compiled with mean annual air temperatures (MAAT) below -1°C to -2°C and annual precipitation of less than 2500 mm (Haeberli 1985), but on a local scale, the topographic and meteorological controls on rockglacier initiation and growth are still not known in detail (Humlum 1998b, 2000). Kirkbride & Brazier (1995) discussed rockglacier formation on a regional scale using qualitative conceptual models and concluded, that the timing of the formation more likely follows the rules of deterministic chaos than corresponds to climatic cooling.

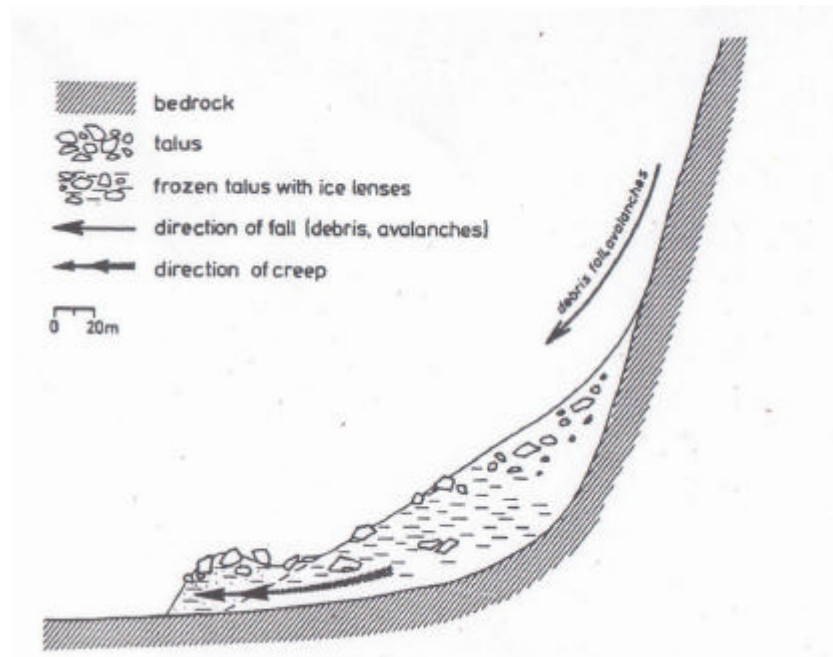


Figure 2.3: Model of the development of talus rockglaciers (below mountain talus slopes) in discontinuous mountain permafrost environments (from Barsch 1996: 186).

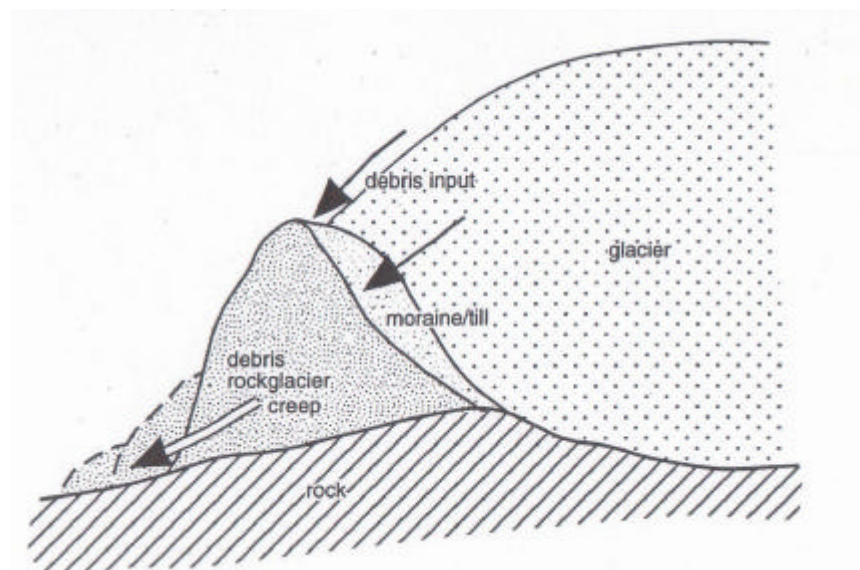


Figure 2.4: Model of the development of a debris rockglacier in mountain permafrost environments (from Barsch 1996: 187).

Rockglaciers are typically situated at the foot of free rock faces (talus rockglacier, figures 2.3, 2.8, 2.10) or below moraines (debris rockglacier, figures 2.4, 2.9) and form tongue- or lobe-shaped bodies with a typical length of 200 – 800 m (Barsch 1996). Normally they are 20-100 m thick; direct means such as coring or indirect means such as geophysical soundings delivered a typical rockglacier thickness of about 50 m (cf., Humlum 2000). A special characteristic are steep lateral and frontal slopes standing at the angle of repose with an apron of coarse blocks at the foot of the slope built by the rockglacier creep (Haeberli 1985). Often, several lobes are superimposed on

each other building a complex topography from different rockglacier generations. These types are called polymorphic bodies, while monomorphic rockglaciers are features without marked surface relief (cf., Frauenfelder et al. 2004).

The rockglacier stratigraphy is described by several authors (e.g., Haeberli 1985; Barsch 1992, 1996; Burger et al. 1999; Humlum 2000; Ikeda & Matsuoka 2002) as a sequence of three main layers: the uppermost 1-5 meters consist of big boulders and are riding on an ice-rich permafrost layer - with 50-70 % of ice and about 30 % of finer-grained material (Barsch 1996) - which is creeping downslope. Below, the third layer consists again of larger rocks, which were deposited at the rockglacier front and subsequently overrun by the other layers. This characteristic sorting of the rockglacier material becomes visible at the rockglacier front. More detailed studies on stratigraphy are delivered by indirect means such as geophysical soundings (e.g., Vonder Mühl 1993; Hauck et al. 2001; Vonder Mühl et al. 2001) or by direct observation in borehole-cores (e.g., Vonder Mühl & Haeberli 1990; Haeberli et al. 1998; Arenson et al. 2002). Burger et al. (1999: 108-109) compiled a comprehensive reference-list of locations, where the internal structure of rockglaciers was investigated.

As derived from four boreholes drilled in 1999, figure 2.5 shows the complex internal structure of the Muragl rockglacier (Arenson et al. 2002). Despite this valuable data, one needs to take into account, that this depicts only local information! The variable distribution of ice layers all over the rockglacier remains speculation.

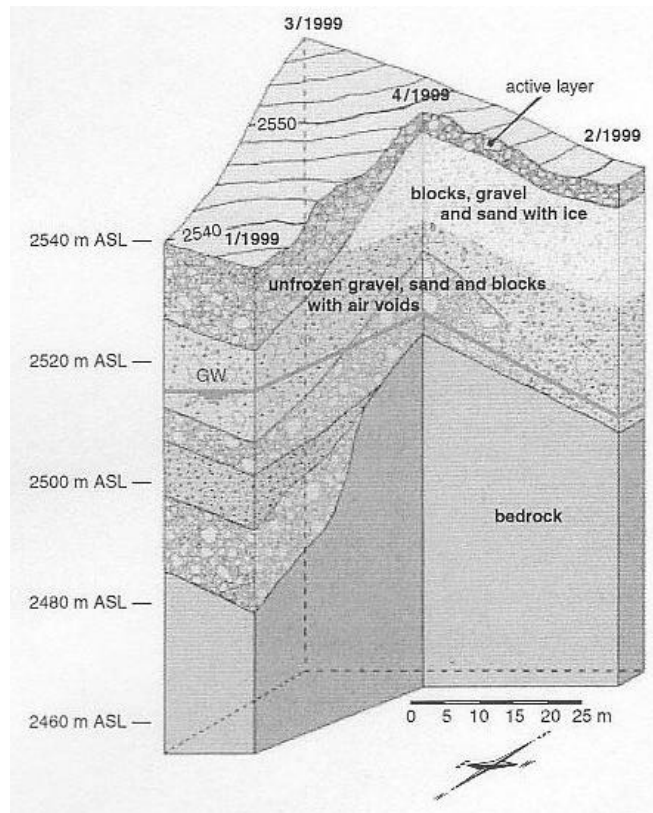


Figure 2.5: Internal structure of the Muragl rockglacier (from Arenson et al. 2002: 122).

The top layer of the permafrost body is typically composed of coarse (0.2 – 5 m) rock fragments (cf., Humlum 1998a) and builds a “*surface relief*” (Humlum 1982) of ridges and furrows which are related to the flow processes, thus, indicating the complex history of rockglacier deformation (Haeberli 1985; Johnson 1992). A detailed description of ‘microrelief on rock glaciers’ is given in Wahrhaftig & Cox (1959). Field measurements and laboratory tests on the development of transverse ridges are discussed in Käab & Weber (2004). In general, it is supposed that transverse ridges and furrows result from compression flow (e.g., Haeberli 1985; Käab et al. 1998). According to Wahrhaftig & Cox (1959) and Barsch (1977), also variations in material supply may lead to the formation of a complex surface topography. Below the furrows subsurface running water is often audible during summer (cf., Elconin & LaChapelle 1997). Other striking but currently not explicable features are small-scale bumps of fine material, probably related to the rockglacier movement.

Additionally, some rockglaciers depict crevasse-like features perpendicular to the flow direction; probably resulting from fast movement such as in steep terrain (e.g., Haeberli & Patzelt 1982). Wahrhaftig & Cox (1959) described these features as tension cracks built by the lateral spreading of the moving mass.

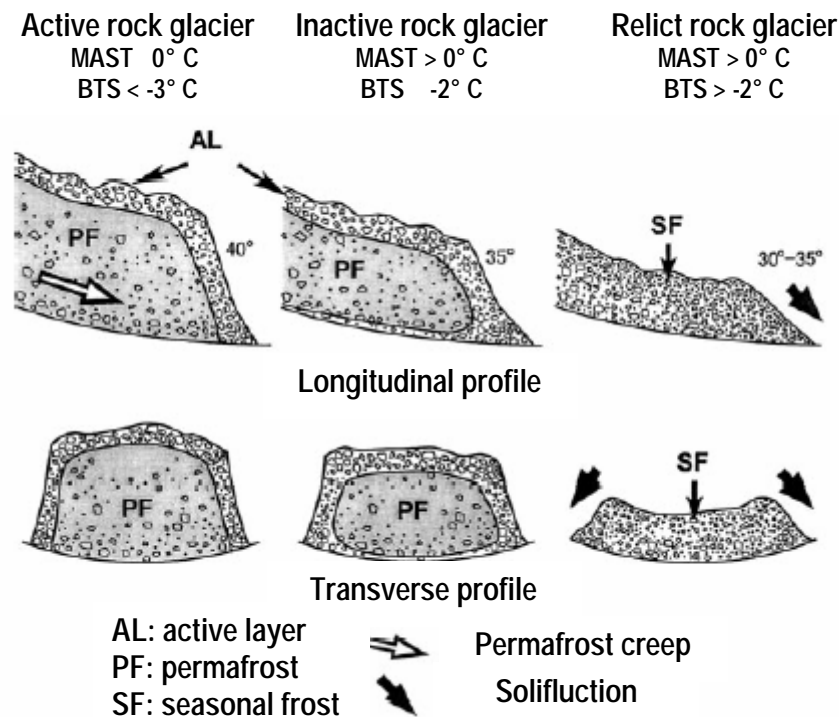


Figure 2.6: Schematic profiles of active, inactive and relict rock glaciers (from Ikeda & Matsuoka 2002: 158).

Due to their ice content and flow behaviour, rockglaciers are classified into the following types: active, inactive and relict. Often they are situated one over the other, forming a sequence of active rockglaciers in higher altitudes to relict rockglaciers in lower altitudes (cf., figure 2.11). A

comparison of morphology, structure and thermal conditions for active, inactive and relict rockglaciers is given in figure 2.6 by Ikeda & Matsuoka (2002). In a strict sense, the activity of rockglaciers is determined e.g., by geodetic survey or photogrammetry, which gives information on their movement. But, in several studies the state of activity has been assessed by morphological characteristics (cf., Wahrhaftig & Cox 1959; Haeberli 1985; Krummenacher et al. 1998; Barsch 1996; Burger et al. 1999; Ikeda & Matsuoka 2002; Nyenhuis et al. in press). Thus, a steep terminal front ($> 35^\circ$) with loose boulders and without vegetation indicates the activity of the feature, whereas inactive rockglaciers, which still contain ice but actually do not move, have a gentler front with stable boulders and partial or full vegetation. Because of their ice content, active and inactive rockglaciers are grouped together as 'intact' rockglaciers (cf., Haeberli 1985). In addition to the morphological approach, the BTS (Bottom Temperature of the winter Snow cover) method is used for the determination of intact rockglaciers and consequently the occurrence of permafrost (Hoelzle 1992; Hoelzle et al. 1999; see chapter 3.5).

Regarding the inactivity of rockglaciers, Barsch (1996) emphasised two causes for inactivation, depending on thermal and mechanical factors (figure 2.7). On one hand the climatic induced inactivity, which is characterised by a thickening of the active layer due to melting of the frozen core and therefore is related to the lower limit of the discontinuous permafrost belt (cf., Ikeda & Matsuoka 2002). In comparison to that, the dynamic induced inactivity results from a reduction in shear stress due to a reduced incorporation of debris and ice or a downslope decrease in slope gradient (Barsch 1996). This kind of inactivation was related only to rockglaciers in continuous permafrost, although a change in debris- and ice-input may occur also in discontinuous permafrost. Olyphant (1987, from Ikeda et al. 2003) made a numerical simulation and confirmed that a decrease in debris input leads to a deceleration of rockglacier advance.

Relict rockglaciers show a collapsed surface due to the melting of the ice. The furrows and ridges are still visible, but the front has a lower angle and the rockglacier surface depicts a dense vegetation cover – at least in areas with fine material (Roer 2001). Relict rockglaciers are valuable indicators for the former permafrost distribution and therefore they are consulted for paleoclimatic reconstructions (cf., Kerschner 1985; Tatenhove & Dikau 1990; Konrad et al. 1999; Frauenfelder & Käab 2000; Frauenfelder et al. 2001). In addition to reconstructions from landform characteristics, different attempts had been made to date rockglaciers with absolute and relative age-determination methods (e.g., Barsch & King 1975; Kirkbride & Brazier 1995; Humlum 1996; Frauenfelder & Käab 2000; Haeberli et al. 2003; Frauenfelder et al. 2004).

Generally, the ecological significance of rockglaciers is reflected in their influence on the water cycle (cf. Haeberli 1985; Krainer & Mostler 2002) as well as in their contribution to sediment transport (cf., Höllermann 1983; Barsch 1996). Barsch (1977) stated that about 20 % of all alpine mass wasting is done by rockglaciers. Additionally, due to their thermal dependency, they depict sensitive indicators for environmental changes.

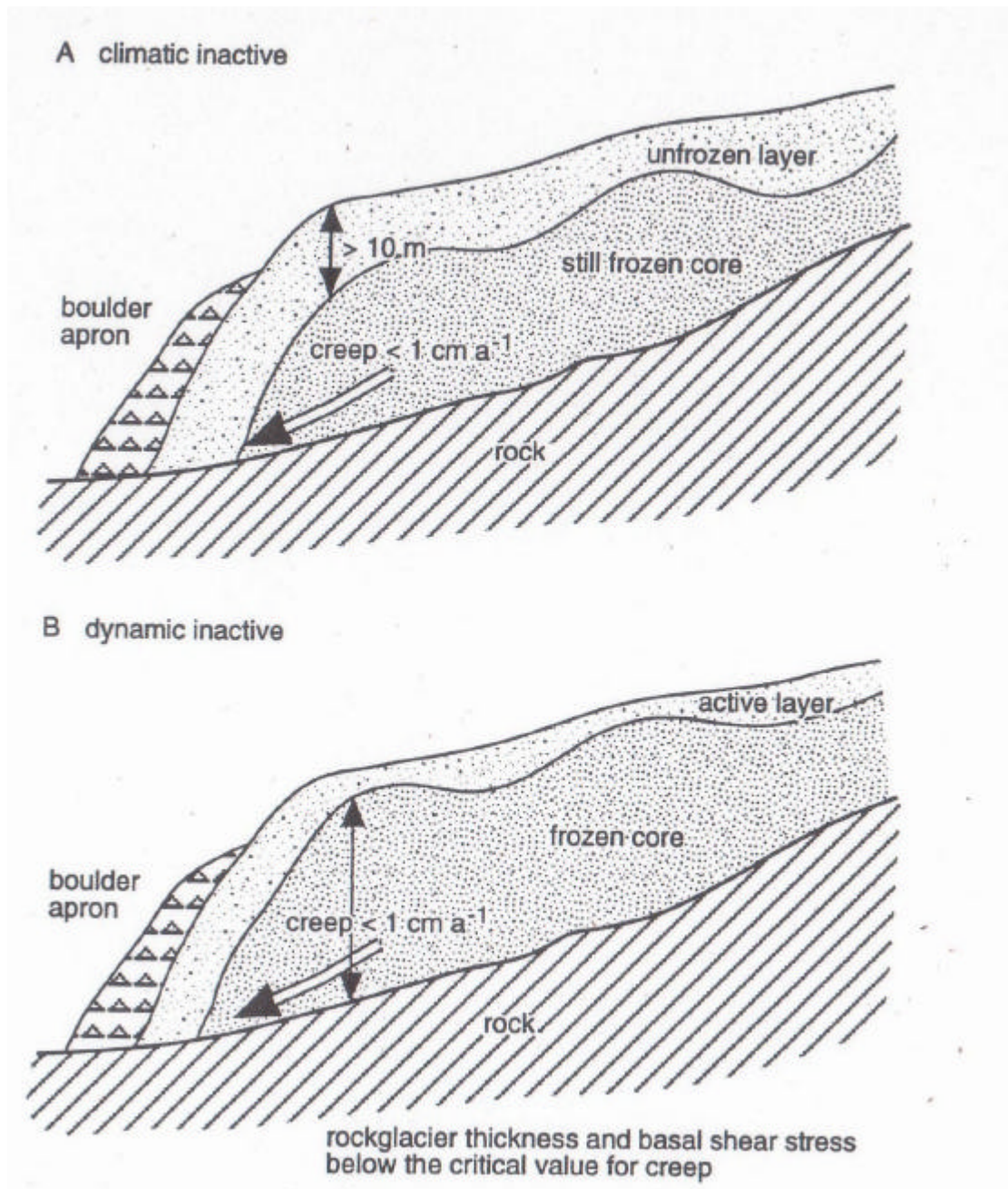


Figure 2.7: Model of inactive rockglaciers. A: Model of a climatic inactive rockglacier. B: Model of a dynamic inactive rockglacier (from Barsch 1996: 193).

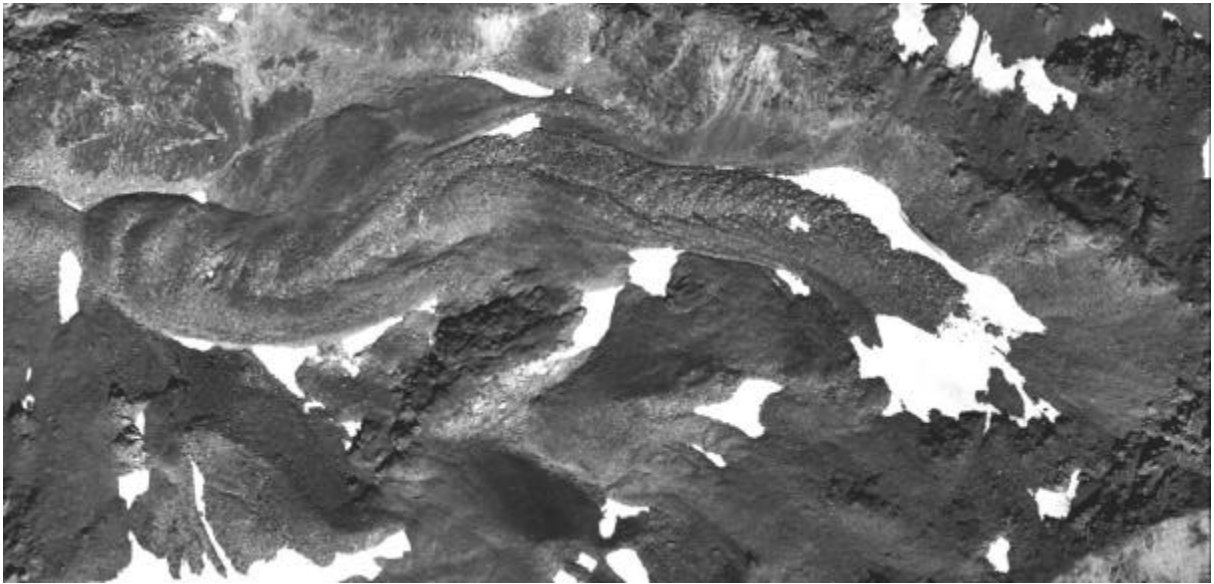


Figure 2.8: Talus rockglacier in discontinuous permafrost at Grueobtalli (Turtmann valley, Switzerland). Underlying orthophoto of 20.08.1993 (flight-line 16, aerial photographs taken by Swisstopo). Plait-like ridge and furrow topography in the upper part of the rockglacier seems to result from sediment input of two different source areas.



Figure 2.9: Debris rockglacier in discontinuous permafrost at Pipjitali (Turtmann valley, Switzerland). Underlying orthophoto of 20.08.1975 (flight-line 22, aerial photographs taken by Swisstopo). Former lateral moraines form the margins of the rockglacier.



Figure 2.10: Talus rockglacier in continuous permafrost at Templet (western Svalbard Archipelago, Norway). Photograph taken in September 2004.

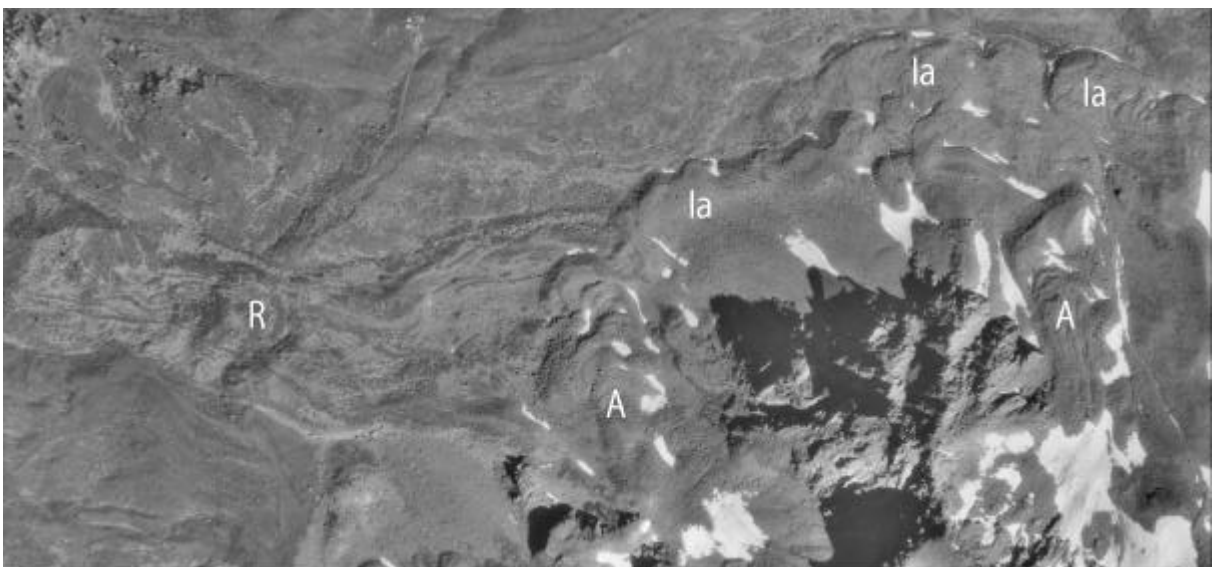


Figure 2.11: Rockglacier sequence in the Hungerlitälli (Turtmann valley, Switzerland); A = active, Ia = inactive and R = relict. Underlying orthophoto of 20.08.1975 (flight-line 22, aerial photographs taken by Swisstopo).

2.3.5 Rockglacier kinematics

Kinematics [greek: kína = movement] is defined as the quantification of movement (velocity, acceleration) without considering the forcing factors (in contrast to dynamics). The velocity is generally described as a vector in a four-dimensional field $\mathbf{v} = (v_x, v_y, v_z)^T$, where x and y represent the coordinates and z depicts the altitude. The horizontal components at the surface are determined by $\Delta x / \Delta t = v_x^s$ and $\Delta y / \Delta t = v_y^s$. Thus, the velocity includes temporal aspects (velocity between the times of the measurements) as well as spatial aspects (velocity between the corresponding points) (Kääb 1996). Against that, **dynamics** [greek: dýnamis = force] involves forces and their interactions as well as the resulting changes in physical systems (based on the second axiom of Newton).

2.3.5.1 Rockglacier movement

For the quantification of rockglacier movement which results from permafrost creep, in general three different components are considered: horizontal velocities, vertical changes and the front advance. Regarding horizontal displacements, rockglaciers move from a few centimetres to one meter per year (Haeberli 1985), generally well below one meter (Whalley & Martin 1992), i.e. at a considerably slower rate than normal glaciers. Barsch (1996) described horizontal velocities between 1-2 cm (minimum) and 100-200 cm (maximum). Higher movements are rare and mostly result from specific topographic conditions (extremely steep gradients). A comprehensive review of published data on rockglacier kinematics (horizontal velocities, vertical velocities and front advance) is given in the appendix 1. In general, the velocities are within the spectrum given by Barsch (see above). Exceptionally fast-moving rockglaciers with velocities of up to 100 m/a are reported from the Andes (Corte 1987) and from Asia (Gorbunov et al. 1992). In the Alps, the highest horizontal velocities (almost 7 m/a) were documented by Chesi et al. (1999) and Krainer & Mostler (2000) for the rockglacier Inneres Reichenkar (Austria). Also the rockglacier Äusseres Hochebenkar (Austria) showed maximum velocities of 5-6 m/a (Vitoris 1972; Schneider 2001). In Switzerland, mean velocities of 2 m/a were measured on Val da l' Aqua rockglacier (Chaix 1943; Jäckli 1978, from Barsch 1992) in Grisons. Highest mean velocities in the Valais are described by Kruppenacher et al. (1998) for the Furggentälti rockglacier (1.35 m/a) and by Strozzi et al. (2004) for the Gruben rockglacier (2 m/a).

Vertical movements may result from diverse processes like 3-dimensional straining (compression, extension), input of debris, formation of ice from snow or water, climatic influences or the advance of individual lobes (for summary see Kääb et al. 2003). All these influences are reflected in the thickening or thinning, respectively, at the rockglacier surface (see chapter 2.3.5.4). The rates are mostly very low and thus often below the level of significance (cf., reference-list in appendix 1). A typical vertical movement of -0.06 m/a was measured by Barsch & Hell (1975) on Murtèl rockglacier (Grison) by means of photogrammetry.

The front advance of rockglaciers is many times lower than the horizontal movement, due to the vertical velocity profile which is indicated by the boulder apron in front of the terminus. Velocities between 0.01 m/a (Murtèl), 0.05 m/a (Muragl) and 0.15 m/a (Gruben) were

monitored by Kääb (1996, 1997) (cf., reference-list in appendix 1). Thus, the values are around 10 % of the corresponding horizontal velocity.

Comparisons of rockglaciers in the European Alps and the polar regions show clear differences in horizontal and vertical velocities as well as front advance, which result from the differences in ground thermal conditions (Kääb et al. 2002, 2003).

2.3.5.2 Spatial variation of movement (surface & depth)

The spatial variation of horizontal velocities mostly reveals highest horizontal velocities in the central flowline while to the borders of the rockglacier the displacement often decreases abruptly (e.g., Barsch 1992, 1996; Roer et al. 2005). Regarding the root zone, it is suggested that the velocities are lower due to a smaller thickness of the deforming layer (Kääb et al. 2003). At the other margins, this phenomenon is due to increased friction which leads to compressing flow (Haeberli 1985). The latter is reflected in the small-scale topography (cf., figure 2.18). In parts where horizontal creep compression takes place, the velocities are in general lower than in parts with extensive flow. Due to mass balance effects horizontal compressive flow is accompanied by vertical extension, which becomes visible in ogive-like transverse ridges. Their downslope movement approximately equals that of the creeping mass (Kääb et al. 1998). In areas of horizontal extension, vertical compression takes place (e.g., Gorbunov et al. 1992). Thus, a close correlation between spatial variations of horizontal and vertical movement exists. Apart from these flow effects, losses and gains of material may influence the mass balance. Kääb et al. (1998) documented changes in rockglacier surface elevation with distinct losses on perennial ice banks and gains in areas with debris accumulation. Due to topographic reasons, these gains and losses are mostly concentrated in the upper part of the rockglacier.

Beside the mass balance effects, the vertical movement is regarded in different ways. On one hand the flow component due to movement parallel to the surface, which amounts to 10-60 % of the horizontal displacement (Haeberli 1985: 87). On the other hand the profile of the movement in depth, where velocity varies according to a parabolic function (Burger et al. 1999). Within the profile, highest velocities occur at the rockglacier surface, thus indicating the cumulative movement of the whole body. But, about 2/3 of the movement is concentrated in a thin - a few metres thick - layer in a certain depth, while the remaining deformation is distributed regularly in the matrix above. This phenomenon is well investigated by borehole deformation measurements (e.g., Vonder Mühl & Haeberli 1990; Wagner 1992; Arenson et al. 2002). Deformation profiles of different rockglaciers are given in figure 2.12.